https://doi.org/10.5194/acp-2020-705
Preprint. Discussion started: 5 October 2020

Atmospheric Chemistry and Physics Discussions

Effects of prescribed CMIP6 ozone on simulating the Southern Hemisphere atmospheric circulation response to ozone depletion

Ioana Ivanciu[1], Katja Matthes[1,2], Sebastian Wahl[1], Jan Harlaß[1], and Arne Biastoch[1,2]

[1]GEOMAR Helmholtz Centre for Ocean Research Kiel, Kiel, Germany
[2]Faculty of Mathematics and Natural Sciences, Christian-Albrechts Universität zu Kiel, Kiel, Germany

Correspondence: Ioana Ivanciu (iivanciu@geomar.de)

Abstract. The Antarctic ozone hole has led to substantial changes in the Southern Hemisphere atmospheric circulation, such as the strengthening and poleward shift of the mid-latitude westerly jet. Ozone recovery during the twenty-first century is expected to continue to affect the jet's strength and position, leading to changes in the opposite direction compared to the twentieth century and competing with the effect of increasing greenhouse gases. Simulations of the Earth's past and future climate, such as those performed for the Coupled Model Intercomparison Project Phase 6 (CMIP6), require an accurate representation of these ozone effects. Climate models that use prescribed ozone fields lack the important feedbacks between ozone chemistry, radiative heating, dynamics, as well as transport. These limitations ultimately affect their climate response to ozone depletion. This study investigates the impact of prescribing the ozone field recommended for CMIP6 on the simulated effects of ozone depletion in the Southern Hemisphere. We employ a new, state-of the-art coupled climate model, FOCI, to compare simulations in which the CMIP6 ozone is prescribed with simulations in which the ozone chemistry is calculated interactively. At the same time, we compare the roles played by ozone depletion and by increasing concentrations of greenhouse gases in driving changes in the Southern Hemisphere atmospheric circulation, using a series of historical sensitivity simulations. FOCI reliably captures the known effects of ozone depletion, simulating an austral spring and summer intensification of the mid-latitude westerly winds and of the Brewer-Dobson circulation in the Southern Hemisphere. Ozone depletion is the primary driver of these historical circulation changes in FOCI. These changes are weaker in the simulations that prescribe the CMIP6 ozone field. We attribute this weaker response to the missing ozone-radiative-dynamical feedbacks and to a prescribed ozone hole that is displaced compared to the simulated polar vortex, altering the propagation of planetary wave activity. As a result, the dynamical contribution to the ozone-induced austral spring lower stratospheric cooling is suppressed, leading to a weaker cooling trend. Consequently, the intensification of the polar night jet is also weaker in the simulations with prescribed CMIP6 ozone. In addition, the persistence of the Southern Annular Mode is shorter in the prescribed ozone chemistry simulations. These results suggest that climate models which prescribe the CMIP6 ozone field still underestimate the historical ozone-induced dynamical changes in the Southern Hemisphere, while models that calculate the ozone chemistry interactively simulate an improved response to ozone depletion.

https://doi.org/10.5194/acp-2020-705
Preprint. Discussion started: 5 October 2020

Atmospheric Chemistry and Physics Discussions

1 Introduction

Anthropogenic emissions of ozone depleting substances (ODS), in particular Chlorofluorocarbons (CFCs), led to a steep decline in stratospheric ozone concentrations since the 1980s. The strongest ozone depletion occured in austral spring above Antarctica. There, the particularly low temperatures inside the winter polar vortex enable the formation of polar stratospheric clouds (PSC). Upon the arrival of sunlight in spring, heterogeneous chlorine photochemistry on the surface of PSC makes chlorine particularly effective in destroying ozone (e.g., Solomon, 1999). As a result, the ozone hole develops every spring in the Antarctic stratosphere, with profound impacts for the Southern Hemisphere (SH) climate. Observations (e.g., Randel and Wu, 1999; Thompson and Solomon, 2002; Randel et al., 2009; Young et al., 2013) and model simulations (Mahlman et al., 1994; Arblaster and Meehl, 2006; Gillett and Thompson, 2003; Stolarski et al., 2010; Perlwitz et al., 2008; Son et al., 2010; McLandress et al., 2010; Polvani et al., 2011; Young et al., 2013; Eyring et al., 2013; Keeble et al., 2014) consistently show a cooling of the Antarctic lower stratosphere in austral spring and summer during the last decades of the twentieth century due to decreased radiative heating as a result of ozone depletion. This cooling led to important changes in the dynamics of the SH. Lower polar cap temperatures resulted in an increased meridional temperature gradient between the cold polar cap and the relatively warmer mid-latitudes. Consequently, the spring stratospheric polar vortex strengthened (Thompson and Solomon, 2002; Gillett and Thompson, 2003; Arblaster and Meehl, 2006; McLandress et al., 2010; Thompson et al., 2011; Keeble et al., 2014) and its breakdown was delayed by about two weeks (Waugh et al., 1999; Langematz et al., 2003; McLandress et al., 2010; Previdi and Polvani, 2014; Keeble et al., 2014). This enabled an intensification of the planetary wave activity propagating into the stratosphere, resulting in an enhancement of the Brewer-Dobson circulation (BDC) in austral summer (Li et al., 2008, 2010; Oberländer-Hayn et al., 2015; Polvani et al., 2018; Abalos et al., 2019).

At the same time, the strengthening of the stratospheric westerlies extended downward affecting the tropospheric jet, which intensified with a lag of one to two months, in austral summer (Thompson and Solomon, 2002; Gillett and Thompson, 2003; Perlwitz et al., 2008; Son et al., 2010; Eyring et al., 2013). The intensification of the stratospheric and tropospheric jets was accompanied by a concurrent positive trend in the Southern Annular Mode (SAM, Thompson and Solomon, 2002; Gillett and Thompson, 2003; Marshall, 2003; Perlwitz et al., 2008; Fogt et al., 2009; Thompson et al., 2011). The surface westerlies strengthened on their poleward side and weakened on their equatorward side, therefore shifting towards higher latitudes during the austral summer (Polvani et al., 2011). This resulted in the poleward displacement of the SH storm track and led to changes in cloud cover (Grise et al., 2013) and precipitation, not only at the high and mid-latitudes (Polvani et al., 2011; Previdi and Polvani, 2014), but also in the subtropics (Kang et al., 2011). The formation of the ozone hole also affected the Antarctic surface temperatures, with East Antarctica experiencing cooling and the Antarctic Peninsula and Patagonia warming (Thompson and Solomon, 2002). Other consequences of the ozone hole formation include the elevation of the SH polar tropopause (Son et al., 2009; Polvani et al., 2011) and the poleward expansion of the Hadley Cell (Garfinkel et al., 2015; Waugh et al., 2015; Polvani et al., 2011; Min and Son, 2013; Previdi and Polvani, 2014) in austral summer. The wind stress over the Southern Ocean, associated with the westerlies, has also experienced a significant strengthening and poleward shift (Yang et al., 2007; Swart and Fyfe, 2012), with implications for the SH ocean circulation. Ocean circulation changes due to the formation of the Antarctic

https://doi.org/10.5194/acp-2020-705
Preprint. Discussion started: 5 October 2020


Atmospheric Chemistry and Physics Discussions

ozone hole include the intensification and poleward shift of the SH supergyre, which connects the subtropical Pacific, Atlantic and Indian Oceans (Cai, 2006), an increase in the transport of salty and warm waters from the Indian into the Atlantic Ocean, known as the Agulhas Leakage (Biastoch et al., 2009, 2015; Durgadoo et al., 2013), and changes in the Ekman transport and upwelling in the Southern Ocean (Thompson et al., 2011 and references therein).

As ozone depletion had such profound implications for the SH climate, accurate model simulations of past and future climate change require a correct representation of stratospheric ozone changes and their associated impacts. Multiple lines of evidence suggest that the method used to specify stratospheric ozone in models affects their response to ozone depletion (Gabriel et al., 2007; Crook et al., 2008; Gillett et al., 2009; Waugh et al., 2009; Haase and Matthes, 2019). Ozone concentrations can be calculated interactively (e.g., Haase and Matthes, 2019), as it is the case in chemistry climate models (CCMs) or can be prescribed, either as zonal means or three-dimensionally (3D, e.g., Crook et al., 2008), as monthly-means or at daily resolution. Ozone asymmetries, the temporal resolution of the prescribed ozone field, as well as feedbacks between ozone, temperature, dynamics and transport all impact the way in which changes driven by decreasing ozone concentrations are simulated. This paper investigates how the lack of ozone-radiative-dynamical feedbacks and the monthly temporal resolution of the prescribed ozone field, recommended for the Coupled Model Intercomparison Project Phase 6 (CMIP6), affect the atmospheric circulation response to ozone depletion in simulations that do not calculate the ozone chemistry interactively.

The position of the Antarctic ozone hole is not centered above the South Pole, but varies with that of the polar vortex, being displaced towards the Atlantic sector in the climatological mean (e.g., Grytsai et al., 2007). As a result, the ozone field is characterized by zonally-oriented asymmetries, henceforth referred to as zonal asymmetries in ozone or ozone waves. The effect of zonal asymmetries in ozone was previously investigated for both hemispheres (e.g., Gabriel et al., 2007; Crook et al., 2008). In the Northern Hemisphere winter, zonally asymmetric ozone alters the structure of the stationary wave one, resulting in temperature changes in the stratosphere and mesosphere (Gabriel et al., 2007; Gillett et al., 2009). Ozone waves were also found to affect the number of sudden stratospheric warmings (SSWs), but studies disagree about the sign of the change (Peters et al., 2015; Haase and Matthes, 2019). Peters et al. (2015) reported an increased number of SSWs and a weakening of the Arctic Oscillation between the mid-1980s and mid-1990s in a simulation with specified zonal asymmetries in ozone compared to one in which zonal mean ozone was prescribed. In contrast, Haase and Matthes (2019) found that fewer SSWs occurred between 1955 and 2019 when zonal asymmetries in ozone were prescribed and even less SSWs occurred when the ozone chemistry was calculated interactively.

In the SH, the largest zonal asymmetries in ozone occur in spring (Gillett et al., 2009; Waugh et al., 2009), when the stratospheric polar vortex is disturbed by the flux of wave activity from the troposphere and when the ozone hole develops. Model simulations that do not include zonal asymmetries in ozone exhibit a warmer lower stratosphere above Antarctica in austral spring and weaker westerly winds during the decades characterized by strong ozone depletion (Crook et al., 2008; Gillett et al., 2009). The effect of zonal asymmetries in ozone on stratospheric temperature, and hence on the polar vortex, is mediated through changes in stratospheric dynamics and cannot be explained solely by changes in radiative heating associated with the ozone field (Crook et al., 2008; Li et al., 2016). In addition to differences in the mean state, trends in temperature and in the strength of the stratospheric and tropospheric westerly jets are underestimated in both past (Waugh et al., 2009; Li

https://doi.org/10.5194/acp-2020-705
Preprint. Discussion started: 5 October 2020


Atmospheric Chemistry and Physics Discussions

et al., 2016; Haase et al., 2020) and future (Waugh et al., 2009) simulations that do not include zonal asymmetries in ozone. Furthermore, as the ocean circulation is sensitive to changes in the surface wind stress, it is also affected by the stratospheric zonal asymmetries in ozone. Weaker spring and summer surface westerlies trends in simulations that prescribe zonal mean monthly mean ozone therefore translate into weaker changes in the SH Ekman transport and in the Meridional Overturning Circulation (Li et al., 2016).

Besides zonal asymmetries in ozone, prescribing monthly mean ozone values that are then linearly interpolated to obtain a higher temporal resolution also leads to differences in atmospheric dynamics compared to simulations using interactive chemistry (Sassi et al., 2005; Neely et al., 2014). Linearly interpolating between prescribed monthly ozone values results in an underestimation of ozone depletion compared to interactive chemistry simulations, as the rapid ozone changes during austral spring cannot be fully captured. The weaker ozone hole, in turn, leads to a warmer lower stratosphere and smaller changes in both the stratospheric and the tropospheric westerly winds. Neely et al. (2014) found that these differences greatly diminish if daily ozone is prescribed instead of monthly mean ozone and concluded that the coarse temporal resolution of the prescribed ozone accounts for the majority of the difference in the austral spring stratospheric temperature and the austral summer stratospheric westerly jet between simulations with prescribed and interactive ozone.

Feedbacks between stratospheric ozone, temperature and dynamics can only occur in models that calculate the ozone chemistry interactively, i.e. in CCMs. Changes in temperature caused by ozone depletion, either directly through radiative cooling or indirectly through changes in dynamics, feed back onto ozone concentrations by altering the rate of the catalytic ozone destruction reactions. At the same time, cooling of the polar caps due to ozone loss enhances the meridional temperature gradient in the stratosphere and, as dictated by the thermal wind balance, strengthens the polar vortices. The stronger westerlies, in turn, impact the upward propagation of planetary waves from the troposphere and therefore lead to changes in the BDC, which transports ozone to high latitudes. Changes in stratospheric dynamics due to ozone depletion thus also feed back onto the ozone concentrations. Haase and Matthes (2019) described one such feedback in the Northern Hemisphere spring, during the break-up of the polar vortex. At this time of the year the westerlies are weak and decreasing ozone levels lead to increased planetary wave forcing. This results in dynamical heating and enhanced ozone transport from the low latitudes, both of which lead to an increase in the ozone concentrations, forming a negative feedback loop. This feedback only occurred in the model simulation in which interactive chemistry was used, and not in the simulations in which either zonal mean or three-dimensional ozone was prescribed, showing the importance of calculating the ozone chemistry interactively. A similar feedback also operates in the SH (Lin et al., 2017).

Previous research thus points to climate models that include interactively calculated ozone chemistry as the preferred choice for studies of past and future climate. However, the computational cost of coupled climate models with interactive chemistry is still very high, especially when long climate simulations are needed, as for CMIP6. Therefore, not all climate models participating in CMIP6 use interactive chemistry, but instead use atmospheric chemistry data sets obtained from simulations with CCMs. The new atmospheric ozone field recommended for use in CMIP6 (Hegglin et al., 2016) is 3D and has monthly temporal resolution. The issue of smoothing ozone extremes by linearly interpolating from monthly values to the model time step still remains in CMIP6. Additionally, the prescribed ozone field, which was generated by different climate models, is not

https://doi.org/10.5194/acp-2020-705
Preprint. Discussion started: 5 October 2020


Atmospheric Chemistry and Physics Discussions

consistent with the dynamics of the models to which it is prescribed and, furthermore, feedbacks between ozone, temperature and dynamics cannot occur. These limitations suggest that there are still differences in atmospheric dynamics between climate models using the prescribed CMIP6 ozone and fully interactive CCMs. In this study, we test this hypothesis for the first time by comparing two ensembles of simulations with the new coupled climate model FOCI (Flexible Ocean Climate Infrastructure, Matthes et al., 2020): one ensemble in which the model uses interactive ozone chemistry and one ensemble in which the CMIP6 ozone is prescribed. We investigate differences in atmospheric dynamics with respect to both the mean state and multi-decadal trends over the second half of the twentieth century and the beginning of the twenty-first century. Details about the climate model FOCI and our methodology can be found in Sect. 2. As the increase in anthropogenic greenhouse gases (GHG) was also reported to lead to changes in the SH circulation (Fyfe et al., 1999; Kushner et al., 2001), we first assess the extent to which the formation of the ozone hole and the increase in GHG contribute to the changes simulated in FOCI in Sect. 3 and we verify the model's ability to correctly simulate the effects of ozone depletion. We then compare the two ensemble simulations and evaluate the performance of the model with prescribed CMIP6 ozone against the interactive chemistry version of the model in Sect 4. Finally, Sect. 5 presents the discussion of the results, together with our conclusion.

2 Model description and methodology

2.1 Model description and experimental design

The coupled climate model employed in this study is the new Flexible Ocean Climate Infrastructure (FOCI, Matthes et al., 2020). FOCI consists of the high-top atmospheric model ECHAM6.3 (Stevens et al., 2013) coupled to the NEMO3.6 ocean model (Madec and the NEMO team, 2016). Land surface processes and sea ice are simulated by the JSBACH (Brovkin et al., 2009; Reick et al., 2013) and LIM2 (Fichefet and Maqueda, 1997) modules, respectively. We use the T63L95 setting of ECHAM6, corresponding to 95 vertical hybrid sigma-pressure levels up to the model top at 0.01 hPa and approximately 1.8° by 1.8° horizontal resolution in the atmosphere. The ocean model, in the ORCA05 configuration (Biastoch et al., 2008), has a nominal global resolution of 1/2° and 46 z-levels in the vertical. FOCI has an internally generated Quasi-Biennial Oscillation (QBO) and includes variations in solar activity according to the recommendations of the SOLARIS-HEPPA project (Matthes et al., 2017) for CMIP6. For the interactive chemistry simulations used in this study, chemical processes were simulated using the Model for Ozone and Related Chemical Tracers (MOZART3, Kinnison et al., 2007), implemened in ECHAM6 (ECHAM6-HAMMOZ, Schultz et al., 2018). A detailed description of FOCI, including the configuration of ECHAM6-HAMMOZ and its chemical mechanism, can be found in the paper by Matthes et al. (2020). A 1500-year long pre-industrial control simulation with FOCI, allowing for the proper spin-up of the model, serves as the starting point for the simulations described below.

Table 1 gives an overview of the simulations used in this study. Three ensembles, each consisting of three simulations differing only in their initial conditions, were conducted in order to distinguish between the effects of ozone depletion and those of increasing GHG concentrations on the SH climate. The first ensemble (REF) comprises of transient simulations in which emissions of both GHG and ODS vary over time according to the historical CMIP6 forcing data set (Meinshausen et al., 2017). Therefore, this ensemble captures the combined effects of ozone depletion and GHG increase. In the second ensemble

https://doi.org/10.5194/acp-2020-705
Preprint. Discussion started: 5 October 2020


Atmospheric Chemistry and Physics Discussions

(NoODS), CO_2 and CH_4 emissions vary according to the historical forcing, but the ODS follow a perpetual seasonal cycle representative of the 1960 conditions, computed for each ODS by taking the mean annual cycle between 1955 and 1965. This ensemble was designed to simulate the effects of increasing GHG in the absence of ozone depletion. Here, we use GHG to refer to CO_2 and CH_4 only, while the other anthropogenic GHG fall under the ODS category. In the third ensemble (NoGHG), the ODS vary according to the historical forcing, while GHG follow a perpetual 1960 seasonal cycle, meaning that there is no increase in GHG past this date. This experimental design allows us to quantify the impact of the formation of the ozone hole by taking the difference between REF and NoODS and that of climate change by taking the difference between REF and NoGHG. All of these sensitivity simulations use the FOCI configuration that includes interactive chemistry, such that the chemical-radiative-dynamical feedbacks are captured and the ozone field is consistent with the simulated dynamics. Additionally, the high resolution ocean nest INALT10X (Schwarzkopf et al., 2019) was used for these simulations. The INALT10X nest enhances the ocean resolution to 1/10° over the South Atlantic Ocean, the western part of the Indian Ocean and over the corresponding Southern Ocean sectors, resolving the mesoscale eddies found in these regions and allowing us to assess, in a follow-up study, the influence of climate change and of ozone depletion on the ocean circulation around the tip of South Africa.

In order to analyze the differences between simulations with interactive ozone chemistry and simulations with prescribed CMIP6 ozone, two further ensembles were performed, each consisting of three simulations differing only in their initial conditions. For the Chem ON ensemble, FOCI was ran in the configuration with interactive chemistry, such that the chemical reactions that are necessary to represent stratospheric chemical processes were included. Therefore, the feedbacks between the stratospheric ozone, temperature and dynamics occur in Chem ON and the simulated ozone field is consistent with the dynamics. A comparison of the ozone field simulated in Chem ON with observations can be found in the work of Matthes et al. (2020). For the Chem OFF ensemble, the ozone field recommended for CMIP6 (Hegglin et al., 2016) was prescribed. The CMIP6 ozone field was generated by two CCMs and includes solar variations from the SOLARIS-HEPPA project (Matthes et al., 2017). It is a monthly-mean, three-dimensional field and therefore includes zonal asymmetries in ozone. The monthly mean values were linearly interpolated and prescribed at each model time step. The comparison of the Chem ON and Chem OFF ensembles sheds light on the impact of prescribing the CMIP6 chemistry on the climate simulated by the coupled climate model FOCI.

2.2 Methodology

We used the transformed Eulerian mean framework (Andrews et al., 1987) to calculate the residual circulation and its forcing. According to the downward control principle of Haynes et al. (1991), the residual downward velocity $\overline{w^*}$ at a certain level is driven by the wave dissipation at the levels above. The divergence of the Eliassen-Palm (EP) flux, $(a\cos\phi)^{-1}\nabla\cdot F$, gives a measure of the dissipation of resolved waves, where

$$\nabla\cdot F = \frac{1}{a\cos\phi}\frac{\partial(F_\phi\cos\phi)}{\partial\phi} + \frac{\partial F_p}{\partial p} \quad (1)$$

https://doi.org/10.5194/acp-2020-705
Preprint. Discussion started: 5 October 2020


Atmospheric Chemistry and Physics Discussions

The components of the EP flux are given by

$$F_\phi = -a\cos\phi\overline{v'u'} \tag{2}$$

$$F_p = fa\cos\phi\frac{\overline{v'\theta'}}{\overline{\theta_p}} \tag{3}$$

The notation is the same as in Andrews et al. (1987): the overbars denote the zonal mean and the primes denote departures from the zonal mean, a is the radius of the Earth, ϕ is the latitude, u and v are the zonal and meridional velocity components, respectively, f is the Coriolis parameter, θ is the potential temperature and θ_p is the partial derivative of θ with respect to pressure. The residual vertical velocity was calculated from the streamfunction, as in McLandress and Shepherd (2009):

$$\overline{w^*} = \frac{gH}{pa\cos\phi}\frac{\partial\Psi}{\partial\phi} \tag{4}$$

where the streamfunction is given by

$$\Psi = -\frac{\cos\phi}{g}\int_p^0 \overline{v^*}(\phi,p)\mathrm{d}p \tag{5}$$

and the meridional residual velocity is given by

$$\overline{v^*} = \overline{v} - \frac{\partial}{\partial p}\left(\frac{\overline{v'\theta'}}{\overline{\theta_p}}\right) \tag{6}$$

with g being the gravitational acceleration and H the scale height taken as 7000 m. The short wave (SW) and long wave (LW) heating rates are part of the standard FOCI output and the total radiative heating rate was obtained by taking the sum of the two. The dynamical heating rate was calculated as the difference between the temperature tendency at daily resolution and the total radiative heating rate.

The SAM was computed as the first empirical orthogonal function (EOF) of the daily, zonal mean geopotential height anomalies at each pressure level, following the method outlined in Gerber et al. (2010). To obtain the geopotential height anomalies, the weighted global mean geopotential height was first subtracted for each day and at each level and latitude. A slowly varying climatology was then removed, to ensure that the resulting SAM index does not exhibit any long-term trend driven by external climate forcing, such that it only reflects internal variability. The slowly varying climatology was obtained by applying a 60-day low pass filter to the geopotential height anomalies from the global mean. Then, timeseries were created for each day of the year and at each location from the filtered anomalies and each timeseries was smoothed using a 30-year low pass filter. The smoothed timeseries were subtracted from the anomalies with respect to the global mean for each respective day and location. The anomalies thus obtained were multiplied by the square root of the cosine of latitude in order to account for the convergence of the meridians towards the poles (North et al., 1982) and only the anomalies for the SH were retained. The first EOF of these anomalies was calculated at each pressure level and the expansion coefficients (principle component timeseries) were obtained by projecting the anomalies onto the first EOF pattern. The expansion coefficients give the SAM index, normalized to have zero mean and unit variance.

https://doi.org/10.5194/acp-2020-705
Preprint. Discussion started: 5 October 2020


Atmospheric Chemistry and Physics Discussions

The SAM e-folding timescale was computed for each day of the year at each pressure level using the method of Simpson et al. (2011). The autocorrelation function (ACF) was obtained by correlating the timeseries for a particular day of the year with the timeseries for the days lagging and leading it. The ACF was smoothed at each lag and pressure level by applying a Gaussian filter with a full width at half maximum of 42 days over a 181 day window. An exponential function was then fitted to the smoothed ACF up to a lag of 50 days using the least squares method and the SAM timescale was obtained by taking the lag at which the exponential function drops to $1/e$.

Linear trends were calculated for the analyzed fields at each level and location and the significance of the trends was assessed based on a Mann-Kendall test. Where differences between simulations are shown, a two-sided t-test was used to test for significance. The significance is always given at the 95% confidence interval. The entire analysis was conducted over the period 1958-2013.

3 Impacts of ozone depletion and climate change on the Southern Hemisphere dynamics

The radiative effects of increasing GHG concentrations lead to cooling of the stratosphere and warming of the troposphere, enhancing the meridional temperature gradient at the tropopause levels, in a similar manner to ozone depletion. While some older studies argued that rising levels of GHG are the driver of the historical dynamical changes in the SH (Fyfe et al., 1999; Kushner et al., 2001; Marshall et al., 2004), at present the general consensus is that the formation of the Antarctic ozone hole is the main cause of these dynamical changes in austral spring and summer and that increasing GHG played only a secondary role (Arblaster and Meehl, 2006; McLandress et al., 2011; Polvani et al., 2011; Keeble et al., 2014; Previdi and Polvani, 2014; World Meteorological Organization, 2018). In this section, we separate the effects of ozone depletion from those of increasing GHG in FOCI and we verify the ability of the model to correctly simulate the dynamical response to ozone loss.

Figure 1 shows the reduction in ozone above the Antarctic polar cap caused by ODS (panel a) together with the accompanying changes in the SW heating rate (panel b). There is a strong decrease in the ozone volume mixing ratio in the lower stratosphere in austral spring, peaking in October, in agreement with previous studies (Perlwitz et al., 2008; Son et al., 2010; Polvani et al., 2011; Eyring et al., 2013). This leads to a significant radiative cooling due to decreased absorption of SW radiation (Fig. 1b). An even stronger SW cooling can be seen above 5 hPa between September and April, in line with the results of Langematz et al. (2003), who found a reduction of the SW heating rate in the upper stratosphere in response to decreasing ozone concentrations. A significant SW warming appears in December and January between 50 and 10 hPa, related to an increased ozone mixing ratio. As will be shown later in this section, these latter changes are attributed to a dynamical response to the spring ozone loss.

Figure 1c shows the ozone changes caused by increasing GHG. There are two regions of statistically significant ozone increase: the upper stratosphere in austral spring and summer and the region of the ozone hole. The SW heating rate (Fig. 1d) exhibits warming in response to increased GHG in the same two regions. As the direct effect of GHG on the SW heating rate is small (Langematz et al., 2003), this warming is likely caused by the higher ozone levels arising in response to the GHG increase, and not directly by the GHG themselves. Higher levels of GHG lead to increased emission of LW radiation

https://doi.org/10.5194/acp-2020-705
Preprint. Discussion started: 5 October 2020


Atmospheric Chemistry and Physics Discussions

(not shown) and have a net cooling effect in the stratosphere. In the upper stratosphere, lower temperatures slow down ozone depletion (Stolarski et al., 2010), explaining the simulated increase in ozone. The ozone increase in the lower stratosphere is more surprising. Here, colder conditions facilitate the formation of PSCs and are therefore expected to enhance ozone loss. Solomon et al. (2015) showed that a cooling of 2 K results in 30 DU more total column ozone loss over Antarctica. Therefore, it does not seem likely that the elevated ozone levels are caused by the radiative effects of GHG. Instead, we find a small but significant enhancement of the downwelling over the polar cap between 50 hPa and 200 hPa in the second half of October, which is associated with increased wave forcing between 20 hPa and 100 hPa (not shown). This suggests that changes in dynamics are responsible for transporting more ozone into the polar lower stratosphere. As a result, the stratospheric ozone depletion is stronger in the absence of increased GHG (NoGHG experiments) than in their presence (REF experiments). The ozone increase related to GHG, about 0.2 ppmv, is, however, small compared to the ozone loss due to ODS, which exceeds 1 ppmv in the region of strongest depletion.

The polar cap temperature response to ozone depletion (Fig. 2a) is closely related to the changes in the SW heating rate shown in Figure 1b. A statistically significant cooling occurs in the lower stratosphere in austral spring and in the upper stratosphere in summer. Additionally, there is a warming above the ozone hole in late spring. It should be noted that the maximum temperature increase above the ozone hole occurs about one month earlier than the maximum shortwave warming, hinting to the fact that it is not a direct radiative effect of the increase in ozone. The temperature decreases are a direct response to ozone depletion. The spring cooling in the lower stratosphere represents the well-known signature of the ozone hole. In contrast to the impact of the ozone hole, there is no significant cooling in the polar lower stratosphere due to increased GHG (Fig. 2c). The cooling resulting from enhanced LW emissions is confined to the upper levels of the stratosphere. The lower stratosphere warms in November in response to GHG. At these levels the SW warming (Fig. 1d) due to the elevated ozone concentrations dominates the LW cooling (not shown) due to GHG, resulting in a net radiative warming.

The zonal wind changes associated with ozone depletion (Fig. 2b) and increasing GHG (Fig. 2d) obey the thermal wind balance. The polar night jet accelerates from October onwards as a consequence of the enhanced meridional temperature gradient caused by ozone loss. The maximum acceleration occurs between November and December (Fig. 2b), concomitant with the strongest cooling (Fig. 2a). This westerly acceleration propagates downwards to the tropospheric eddy-driven jet and reaches the surface in November and December. Figure 3a shows the ozone-induced change in the surface zonal wind for these months. The surface westerlies strengthen on their poleward side and weaken on their equatorward side, shifting poleward. This shift is accompanied by changes in sea level pressure (SLP). The pressure over Antarctica drops significantly and the mid-latitude SLP increases in response to ozone depletion (Fig. 3c), signaling a change towards the positive phase of the SAM. All these changes in the SH dynamics simulated in FOCI in response to ozone depletion, both in the stratosphere and in the troposphere are in good agreement with the results of previous studies that isolated the impacts of ozone loss from those of the increase in GHG (Arblaster and Meehl, 2006; McLandress et al., 2010, 2011; Polvani et al., 2011; Keeble et al., 2014). This demonstrates that FOCI is able to realistically capture the effects of ozone depletion and is therefore suited to study how prescribing the CMIP6 ozone affects the simulated climate response to ozone loss.

https://doi.org/10.5194/acp-2020-705
Preprint. Discussion started: 5 October 2020


Atmospheric Chemistry and Physics Discussions

The response of the stratospheric westerlies to higher GHG concentrations is markedly different from that to ozone depletion (Fig. 2b, d). Driven by the warming over the polar cap, the polar night jet weakens in November. This change is much weaker compared to that resulting from ozone loss and is confined to the stratosphere, lasting for only one month. While GHG do not cause an acceleration of the polar night jet in FOCI, there is a significant positive change in the zonal wind strength centered around 30°S, extending from the top of the eddy-driven jet into the middle stratosphere (supplementary Fig. S1). This westerly change implies a strengthening of the upper flank of the tropospheric jet, in agreement with the findings of McLandress et al. (2010). At the surface, the only significant strengthening of the westerlies occurs in May (Fig. 2d). Figure 3b shows a map of the annual mean GHG-induced changes in the surface zonal winds. We show the annual mean change due to GHG and not the November-December change, as it was the case for ozone depletion because, unlike the effects of ozone loss, the effects of increasing GHG do not exhibit any seasonality. Although the GHG-induced pattern of zonal wind change is similar to that caused by ozone depletion, the changes are much weaker and mostly insignificant. This indicats that the magnitude of GHG increase was not large enough to induce a strong strengthening or poleward shift of the surface westerly winds. The SLP response to increasing GHG exhibits a significant increase in the mid-latitudes, over the South Pacific and Indian Oceans, but the magnitude of this increase is less than half of that due to ozone loss and there is no significant SLP decrease over the polar cap.

Our sensitivity experiments confirm that the changes in the SH polar night jet (Fig. 2b, d) and eddy-driven jet (Fig. 3a, b) during the later part of the twentieth century were mainly driven by ozone depletion. Increasing GHG have played only a minor role, acting to enhance the effect of the ozone hole in the troposphere and to partially counteract the impact of ozone loss on the polar night jet. In addition, we found that the upper stratosphere has cooled significantly and the troposphere has warmed significantly in response to increasing concentrations of GHG.

Having distinguished the contributions of ozone loss and rising GHG levels to the changes in the westerly winds, we now turn our attention to the impacts of ozone depletion on the BDC. Figure 4 shows the November ozone-induced changes in the residual circulation, which is commonly used as a proxy for the BDC. The residual circulation is primarily forced by the dissipation of vertically propagating planetary waves from the troposphere. Therefore, we also present in Figure 4 the changes in eddy heat and momentum fluxes, which reveal the direction of wave propagation, and the changes in the divergence of the EP flux, which measures the wave forcing. The EP flux divergence (Fig. 4c) is characterized by a significant negative change above 10 hPa (stronger convergence) and a significant positive change (weaker convergence) in the lower stratosphere, below 50 hPa. This implies a reduction of wave dissipation in the lower stratosphere and an increase above, suggesting that atmospheric waves propagating from the troposphere reach higher into the stratosphere. This is confirmed by the strengthening of the eddy heat flux above 50 hPa (Fig. 4a). The eddy heat flux is equivalent to the vertical component of the EP flux and gives a measure of the vertical propagation of resolved waves. This strengthening entails increased wave propagation in the middle and upper stratosphere. Similarly, the eddy momentum flux exhibits a negative change, implying increased equatorward wave propagation (Fig. 4b). The ability of the waves to propagate deeper into the stratosphere is related to the strengthening of the polar night jet in response to ozone depletion. Enhanced westerly velocities in November lead to a delay in the breakdown of the polar vortex (e.g., Waugh et al., 1999; Langematz et al., 2003) and sustain wave activity. McLandress et al. (2010) showed

https://doi.org/10.5194/acp-2020-705
Preprint. Discussion started: 5 October 2020


Atmospheric Chemistry and Physics Discussions

that, as a result of ozone depletion, 1) the height of the transition between westerly and easterly velocities has increased, implying that waves can propagate higher at the end of spring, and 2) the date of this transition has been delayed by 10 to 15 days, implying that the period during which waves can penetrate into the stratosphere has been prolonged. As a result, the wave drag due to the dissipation of resolved waves increased in the upper stratosphere and decreased in the lower stratosphere in November (Fig. 4c), while it increased in the lower stratosphere in December (supplementary Fig. S2), driving similar changes in the residual circulation. In November, the residual meridional velocity (Fig. 4d) shows a significant poleward intensification above 20 hPa and a significant weakening below 50 hPa, in good agreement with the changes in the EP flux divergence. The downwelling over the polar cap is enhanced above 50 hPa (Fig. 4e). Associated with this intensification is a large dynamical warming (Fig. 4f) that increases the temperature above the ozone hole, as shown in Fig. 2a, consistent with the results of Mahlman et al. (1994), Li et al. (2008), Stolarski et al. (2010), Keeble et al. (2014) and Ivy et al. (2016). At the same time, the strengthening of the residual circulation transports more ozone to the polar regions, leading to the increase in ozone seen in December between 50 hPa and 10 hPa in Fig. 1a. The residual vertical velocity in the lower stratosphere is expected to weaken in response to the decreased wave drag seen in Fig. 4c below 50 hPa. Such a weakening is simulated in FOCI at 200 hPa (Fig. 4e), accompanied by a decrease in dynamical heating (Fig. 4f). However, the lower stratospheric change in downwelling is not significant at the 95% confidence interval and the change in the dynamical heating is only partly significant. The decrease in austral spring lower stratosphere downwelling was previously reported by Li et al. (2008), McLandress et al. (2010) and Lubis et al. (2016), while the decrease in dynamical heating was shown by Keeley et al. (2007), Orr et al. (2013) and Lubis et al. (2016). Consistent with our results, McLandress et al. (2010) also attributed their weaker downwelling to reduced wave drag in the austral spring. We note that Figure 4 displays changes averaged for the entire month of November. However, the analysis of Orr et al. (2012, 2013) using 15-day averages showed that, at this time of the year, changes in the lower stratosphere wave driving and dynamical heating due to ozone depletion occur over a shorter time. Therefore, it is likely that our November averaging is applied over periods exhibiting changes of different sign, consequently diminishing the magnitude of the change and rendering it insignificant. At the same time, the large internal variability in FOCI makes it hard to discern this change using fields with higher temporal resolution and more ensemble members would be needed to clearly detect the weakening in downwelling.

The temporal evolution of the ozone-driven changes in wave forcing and, as a result, in the residual circulation can be seen by comparing Fig. 4 with supplementary Fig. S2, which shows the same quantities, but for December. It is clear that there is a downward propagation of the changes in all quantities from November to December. As the polar vortex breaks down at the upper levels, the zonal velocities remain westerly below 50 hPa (contours in Fig. 2b) and are still able to support the remnant wave propagation. Stronger westerlies in the lower stratosphere in December imply enhanced wave dissipation. As a result, the downwelling is accelerated in the lower stratosphere, driving dynamical warming there. These results are consistent with those of McLandress et al. (2010) and explain the reason behind the change in the sign of the residual vertical velocity trends in the lower stratosphere between spring and summer.

Our results clearly show that ozone depletion had a significant influence on the SH BDC in austral spring and summer. FOCI simulates little significant residual circulation changes in the SH due to increasing GHG. Therefore, we conclude that

https://doi.org/10.5194/acp-2020-705
Preprint. Discussion started: 5 October 2020


Atmospheric Chemistry and Physics Discussions

the historical changes in the SH residual circulation over the period of ozone depletion are a consequence of the formation of the ozone hole, in line with the findings of Keeble et al. (2014), Oberländer-Hayn et al. (2015), Polvani et al. (2018), Li et al. (2018), Abalos et al. (2019) and the most recent Scientific Assessment of Ozone Depletion (World Meteorological Organization, 2018). Consistent with these studies, FOCI simulates a strengthening of the SH residual circulation in response to enhanced wave forcing at the end of the spring and the beginning of summer. At the same time, a weakening of the spring lower stratosphere residual circulation is simulated, as found by the few studies that investigated springtime changes in the BDC (Li et al., 2008; McLandress et al., 2010; Lubis et al., 2016). The good agreement with previous studies demonstrates that the interactive chemistry configuration of FOCI adequately simulates the impact of ozone depletion on the residual circulation.

4 Effects of prescribing the CMIP6 ozone field

We aim to understand how prescribing the ozone field recommended for CMIP6 affects the SH atmospheric circulation response to ozone depletion. To this end, we compare an ensemble of simulations using prescribed CMIP6 ozone with an ensemble of simulations that use fully interactive chemistry. The use of an ozone field that is not consistent with the model dynamics, the lack chemical-radiative-dynamical feedbacks and the temporal interpolation from the monthly prescribed values to the model time step can all lead to differences between the two ensembles. With a view on these deficiencies, we begin by analyzing the differences in the mean state in Sect. 4.1 and we then compare the simulated SH variability in Sect. 4.2 and the persistence of the SAM in Sect. 4.3.

4.1 Effects on the mean state

Figure 5 shows the difference between Chem ON and Chem OFF in October average ozone and November average temperature, geopotential height and zonal wind at 70 hPa. The CMIP6 ozone field was used for Chem OFF. FOCI simulates significantly lower ozone levels above the Antarctic Peninsula and the Bellingshausen Sea in October compared to the CMIP6 ozone (Fig. 5a). As a consequence, the November temperature (Fig. 5b) and the geopotential height (Fig. 5c) are also lower in this region in Chem ON compared to Chem OFF. We note that the pattern of the temperature difference between Chem ON and Chem OFF is markedly different to the pattern reported by Crook et al. (2008) and Gillett et al. (2009), which arises due to zonal asymmetries in ozone. The CMIP6 ozone field prescribed in Chem OFF includes ozone asymmetries and their effects are therefore captured in Chem OFF. Despite this, spatial temperature and geopotential height differences still remain between simulations with prescribed ozone asymmetries and simulations with fully interactive ozone chemistry.

The differences between the FOCI and the CMIP6 ozone fields are not confined just to the ozone hole itself. Outside of the polar vortex, Chem ON exhibits significantly higher ozone levels at all longitudes. The difference in ozone maximizes in the eastern hemisphere, as the polar vortex, and hence the ozone hole, is not centered over the pole, but displaced towards the Atlantic Ocean and South America (contours in Fig. 5a). This significant positive difference was found in the mid- to high-latitudes of both hemispheres and in all seasons (not shown). We hypothesize that it is the result of a stronger BDC in FOCI compared to the models used to generate the CMIP6 ozone field, leading to increased ozone transport from the

https://doi.org/10.5194/acp-2020-705
Preprint. Discussion started: 5 October 2020


Atmospheric Chemistry and Physics Discussions

tropics. Associated with the higher ozone levels, the November mid-latitude temperature and geopotential height are also elevated in Chem ON compared to Chem OFF. In the Atlantic and Indian sectors, the higher temperature outside of the polar vortex in Chem ON enhances the meridional pressure gradient between the polar low and the mid-latitude high. In the Pacific sector, the meridional pressure gradient is stronger in Chem ON due to the lower temperature above West Antarctica and the Bellingshausen Sea. As a result, the November polar night jet is circumpolarly stronger in Chem ON compared to Chem OFF (Fig. 5d).

To better understand the cause of the lower ozone levels above the Antarctic Peninsula and the Bellingshausen Sea in Chem ON, Figure 6c shows the October average ozone anomalies from the zonal mean in Chem ON at 70 hPa, as well the difference to Chem OFF. A zonal wavenumber one pattern is clearly visible, with the ridge at the edge of Antarctica towards New Zealand and the trough over the tip of the Antarctic Peninsula. The ozone wave simulated in FOCI is consistent with that inferred from satellite observations by Lin et al. (2009) and Grytsai et al. (2007), from reanalyses by Crook et al. (2008) and with that simulated by Gillett et al. (2009). This wave pattern confirms that the simulated ozone hole is not centered on the south pole. While the CMIP6 ozone hole is also displaced from the pole, its location and extent is not the same as that simulated by FOCI (compare contours in Fig. 7a and d). The difference shown in Figure 6c reveals that, on the one hand, the trough of the wave is shifted towards South America and reaches deeper into the Pacific sector in Chem ON. On the other hand, the amplitude of the wave is significantly greater in Chem ON (compare also contours in Fig. 8a and b). Figure 6c thus demonstrates that the prescribed CMIP6 ozone field is not spatially consistent with the polar vortex simulated in FOCI.

Figures 6a and 6b show the time evolution of the ozone wave averaged between 60°S and 70°S for the month of October for Chem ON and Chem OFF, respectively. Despite considerable interannual variability, the westward shift of the wave in Chem ON compared to that in Chem OFF is clearly discernable. Both ozone fields exhibit a deepening of the wave pattern over time, in particular in the 1980s, as the ozone hole becomes stronger, in agreement with the increase in the ozone wave amplitude reported by Grytsai et al. (2007) and Crook et al. (2008). In addition, there is a slow eastward shift of the wave with time, consistent with the phase shift based on temperature observations reported by Lin et al. (2009). An eastwards shift of the ozone zonal wave one was also inferred from satellite observations by Grytsai et al. (2007), accompanied by a westward shifting zonal wave number two. Due to the superposition of the two wave numbers, only the through of the wave sum shifted eastward, while the ridge remained stationary. In our analysis, both the through and the peak exhibit a phase shift. This shift is stronger in Chem OFF (Fig. 6b) and less evident in Chem ON (Fig. 6a).

The consequences of prescribing an ozone field that is not consistent with the model dynamics are depicted in Fig. 6d and e. The wave one pattern can be seen in both temperature and geopotential height anomalies from the zonal means in October. In both fields there are significant differences between Chem ON and Chem OFF. Consistent with the ozone anomalies, the temperature trough is shifted westward in Chem ON and the amplitude of the wave is stronger. The radiative effects of a prescribed ozone hole that is not collocated with the polar vortex appear to alter the location of the wave, while the weaker amplitude of the prescribed ozone wave affects the amplitude of the temperature response. The westward shift of the Chem ON wave is also seen in the geopotential height field (Fig. 6e). We thus conclude that prescribing the CMIP6 ozone field, which is not consistent with the model dynamics in general and with the simulated stratospheric polar vortex in particular, gives rise to

https://doi.org/10.5194/acp-2020-705
Preprint. Discussion started: 5 October 2020


Atmospheric Chemistry and Physics Discussions

425 significant differences in the spatial structure and the amplitude of the springtime lower stratospheric wave one, as well as to significant differences in the springtime climatological strength of the polar night jet. Although we presented here evidence for the 70 hPa level, the results hold true for levels throughout the lower and middle stratosphere.

4.2 Effects on the simulated Southern Hemisphere variability

4.2.1 Temperature

430 We now turn our attention to the differences in the trends simulated by the two ensembles in response to ozone depletion. First, we compare the October 70 hPa ozone trends between Chem ON and Chem OFF (Fig. 7a, d), as they are at the root of the polar stratospheric temperature changes. We also examine the eddy contribution to these trends, i.e. the trends in the anomalies from the zonal mean (Fig. 8a, b). The Chem OFF ozone is given by the prescribed CMIP6 ozone field.

The spatial extent of ozone depletion is greater in Chem ON compared to Chem OFF, but in both cases the ozone trend 435 maximizes over East Antarctica (Fig. 7a, d). The maximum ozone depletion is somewhat stronger in Chem OFF than in Chem ON. The trends in ozone anomalies from the zonal mean exhibit a wave one structure, but the wave is shifted eastwards compared to its climatological position in both ensembles (Fig. 8a, b). This implies a progressive eastward migration of the wave structure over time and an increase in the amplitude of the wave, in agreement with Fig. 6. The locations of the October trend minimum over the Atlantic sector and of the trend maximum over the Pacific sector are consistent with observations (Lin 440 et al., 2009).

There are notable differences between the eddy component of the ozone trends in Chem ON and Chem OFF. The position of the trough is farther east in Chem OFF, while the ridge extends over the Drake Passage, crossing into the Atlantic sector. The ridge of the trend wave is stronger in Chem ON than in Chem OFF. These differences in the trends of the ozone fields passed to the radiation scheme in the two ensembles translate into differences in temperature trends between them. Similarly to the 445 trend in ozone, the eddy component of the temperature trend exhibits a wave one structure which is shifted eastward in Chem OFF compared to Chem ON, albeit less than in the case of ozone (Fig. 8c, d). The eastward displacement of the temperature trend pattern in Chem OFF shows that prescribing an ozone field inconsistent with the dynamics of the model to which it is prescribed alters the spatial structure of the temperature trend.

Even larger differences appear when the full polar temperature trends are compared (Fig. 7b, e). Despite its slightly stronger 450 ozone trend (Fig. 7a, d), Chem OFF displays a considerably weaker temperature trend over the entire Antarctic continent. The trend in the SW heating rate (supplementary Fig. S3) is stronger in Chem OFF than in Chem ON, consistent with the trends in the respective ozone fields (Fig. 7a, d). The net radiative contribution to the temperature trend is weaker in both experiments due to the partial cancelation of the SW cooling and LW warming trends (not shown). Nevertheless, the stronger SW heating trend in Chem OFF demonstrates that the temperature trend differences between Chem ON and Chem OFF cannot 455 be explained by the linear interpolation of the monthly CMIP6 ozone field to the model time step, as it was the case in the studies by Sassi et al. (2005) and Neely et al. (2014). If that were the case, the smaller ozone extremes resulting from the interpolation would also reduce the Chem OFF SW heating rate trend, not just the temperature trend. The key to the different

https://doi.org/10.5194/acp-2020-705
Preprint. Discussion started: 5 October 2020


Atmospheric Chemistry and Physics Discussions

temperature trends in Chem ON and Chem OFF lies instead in the dynamical heating rate trends (Fig. 7c, f). In Chem ON, there is a strong and significant dynamical cooling trend in October over the majority of the Antarctic continent, peaking over East Antarctica (Fig. 7f). This greatly amplifies the lower stratospheric temperature trend due to the radiative heating rate. In Chem OFF, the October dynamical cooling trend over East Antarctica is much weaker and it is not significant, while over West Antarctica a warming trend is visible (Fig. 7c). Consequently, the dynamical heating rate in Chem OFF brings a negligible contribution to the temperature trend, explaining the considerably weaker cooling in this ensemble. The strongest dynamical cooling trend in Chem OFF occurs over the Atlantic sector of the Southern Ocean. The dynamical heating rate is closely related to the polar downwelling, which is, in turn, controlled by the wave dissipation above. Therefore, the different October dynamical cooling trend patterns in Figs. 7c and f have two implications: 1) that wave dissipation is suppressed and 2) that the downwelling weakens in completely different regions in the two ensembles. The cause of these spatial discrepancies is the spatial inconsistency between the prescribed ozone hole and the simulated polar vortex in Chem OFF.

The temperature trends are weaker in Chem OFF not only in October and not only at 70 hPa, but throughout the entire spring and throughout the lower stratosphere (Fig. 9a, b). Comparing the seasonal cycle of the temperature in Chem ON and Chem OFF with the temperature trends derived from three radiosonde data sets depicted in Fig. 2 of the study by Young et al. (2013), it is clear that the trends in Chem ON agree better with the observed trends, while Chem OFF underestimates these trends by about 40%. The warming above the ozone hole in November and December is also weaker in Chem OFF. As shown in Sect. 3, this warming is attributed to changes in the strength of the BDC. Its different magnitude between Chem ON and Chem OFF thus points to the role played by the dynamics in setting the different responses to ozone depletion in the two model configurations. In contrast, the magnitude of the cooling at the stratopause levels in winter and fall is similar between Chem ON and Chem OFF, as this cooling is a purely radiative effect of ozone loss and increase in GHG (Sect. 3).

To illustrate the temporal evolution of the lower stratospheric polar cap temperature in Chem ON and Chem OFF, Fig. 10 shows timeseries of the temperature anomalies with respect to the daily 1958-2013 mean for each austral spring day at 100 hPa. Both ensembles are characterized by large interannual variability. The anomalies switch sign in the 1980s, as the pre-ozone hole decades were warmer than the average, while the decades exhibiting a strong ozone hole were colder than the average, in line with the trends shown in Figs. 7 and 9. Comparing years of temperature minima, Chem ON shows stronger minima than Chem OFF. The same holds true for the temperature maxima. Given the results of Sassi et al. (2005) and Neely et al. (2014), it could be concluded that the reason for the larger extremes in Chem ON is the temporal interpolation applied in Chem OFF, which reduces the extremes. However, when comparing the timeseries of the SW heating rate anomalies (Fig. 10b, d), it becomes evident that this is not the case. The Chem OFF SW heating rate exhibits extremes as large as those in Chem ON. Furthermore, in Chem OFF there are overall more years with strong positive anomalies during the first decades and more years of strong negative anomalies during the later decades, in line with a stronger SW heating trend (supplementary Fig. S3). Note that the smooth transition between the spring months in Chem OFF is the result of the linear interpolation between monthly ozone values. Figure 10 demonstrates that is not just the temperature trend that is stronger in Chem ON, but also individual years are characterized by stronger anomalies in the polar lower stratosphere and that these stronger anomalies cannot be explained by the radiative heating rates. Instead, the feedbacks between ozone, temperature and dynamics in Chem

https://doi.org/10.5194/acp-2020-705
Preprint. Discussion started: 5 October 2020


Atmospheric Chemistry and Physics Discussions

ON lead to the consistent development of the polar vortex and the ozone hole and amplify the temperature anomalies through the effect of the dynamics, as evident from Fig. 7.

4.2.2 Zonal winds

The magnitude of the circumpolar westerly winds trends in Chem ON and Chem OFF is consistent with the magnitude of the temperature trends. A stronger lower stratosphere cooling in Chem ON implies a more pronounced enhancement of the meridional temperature gradient and hence a stronger acceleration of the westerly winds (Fig. 9c, d). The zonal wind trend in Chem ON is not only stronger, but it also occurs about half a month earlier than in Chem OFF, from the end of September onwards. In addition, the timing of the downward propagation of the zonal wind trends to the troposphere also differs. Figure 11 shows the seasonal cycle of the 850 hPa zonal wind trends as a function of latitude. A significant poleward intensification of the tropospheric westerlies can be seen from November through January in Chem ON, accompanied by a deceleration on the equatorward side. In contrast, the westerly winds in Chem OFF exhibit significant trends on both flanks only starting in December and the trends remain significant throughout February. Figure 11 also shows maps of the zonal wind trends at 850 hPa averaged over December and January, the two months in which both ensembles exhibit significant trends in the troposphere. The trends are a circumpolar feature and are characterized by strengthening on the poleward side and a weakening on the equatorward side of the tropospheric jet, implying that the jet has sifted poleward in both ensembles. The shift is, however, stronger in Chem ON than in Chem OFF, in line with the stratospheric trends. Our results offer a possible explanation for the reason why Swart and Fyfe (2012) found that CMIP5 models underestimate the trends in the SH surface wind stress compared to reanalyses, as many of the CMIP5 models prescribed ozone chemistry instead of calculating it interactively. We suggest that using interactive chemistry would improve the representation of the SH westerly wind trends and the associated trends in surface wind stress in climate models.

4.2.3 Mechanisms for the different responses to ozone depletion

To obtain a clear understanding of the dynamical mechanisms responsible for the temperature and zonal wind trend differences between Chem ON and Chem OFF, we investigate the trends in the residual circulation and its drivers. Figure 12 shows vertical profiles of the November trend in the eddy heat flux, the divergence of the EP flux, the vertical and the meridional components of the residual circulation. Trends for October and December have additionally been examined, but are not shown. The October and November dynamical heating rate trends are illustrated in Fig. 13.

We first focus on the different onset dates of the westerly wind trends. A significant positive trend can be seen in the middle and upper stratosphere in Chem ON already at the beginning of October (Fig. 9c), but it only appears in the second half of October in Chem OFF (Fig. 9d). There is also a significant cooling visible in the polar cap middle stratosphere at the beginning of October in Chem ON (Fig. 9a). As this trend occurs above the ozone hole, it is likely the result of dynamical rather than radiative changes. At the beginning of October, the westerly velocities in the polar night jet (contours in Fig. 9c, d) are close to the critical velocity for Rossby wave propagation (Charney and Drazin, 1961). The positive trend (Fig. 9c) is enhancing the winds past this critical velocity and it inhibits wave propagation in Chem ON. A significant decrease in wave dissipation in the

https://doi.org/10.5194/acp-2020-705
Preprint. Discussion started: 5 October 2020


Atmospheric Chemistry and Physics Discussions

lower and middle stratosphere occurs in October in Chem ON, but not in Chem OFF (not shown). This October reduction in wave forcing in Chem ON is consistent with the findings of McLandress et al. (2010), who also used a CCM in their study. The reduced wave forcing has two effects: first, less easterly momentum is deposited through wave dissipation, further enhancing the westerly winds. Second, the polar cap downwelling in the lower stratosphere is weakened due to the decreased wave forcing above, leading to a significant dynamical cooling. A significant October polar cap dynamical cooling trend occurs in the lower stratosphere only in Chem ON and it is absent in Chem OFF (Fig. 13a, b). The lack of a dynamical cooling trend in Chem OFF is explained by the missing feedbacks between ozone and dynamics in this ensemble and by a prescribed ozone hole that is not consistent with the dynamics, as demonstrated above. The dynamical cooling in Chem ON reinforces the negative temperature trend due to the radiative effects of ozone loss and further strengthens the westerly winds via the thermal wind balance, resulting in stronger temperature and zonal wind trends compared to Chem OFF.

In November, the polar vortex breaks down and climatological easterly winds occur in the upper and middle stratosphere (contours in Fig. 9c, d). The positive zonal wind trend prolongs the life of the polar vortex, delaying its breakdown (e.g. McLandress et al., 2010) and allowing planetary waves to propagate higher into the stratosphere, as shown by the negative trend in the eddy heat flux (Fig. 12a, e). Wave dissipation is enhanced in the middle and upper stratosphere and decreased in the lower stratosphere in both Chem OFF and Chem ON (Fig. 12b, f), but the magnitude of the Chem ON trends is larger. In addition, the region of enhanced wave dissipation extends farther down in Chem OFF, confining the region of reduced wave dissipation to the levels below 100 hPa. This has important implications for the residual circulation trends. In Chem OFF, the negative trend in the polar cap downwelling reaches all the way into the lower stratosphere (Fig. 12c). The accompanying polar cap dynamical warming trend (Fig. 13d) partly offsets the radiative cooling trend due to ozone depletion, resulting in the weaker temperature trend seen in Fig. 9b. In contrast, the polar downwelling in Chem ON strengthens only above 50 hPa and exhibits an insignificant weakening below (Fig. 12g). The meridional residual velocity follows a similar pattern, strengthening in the upper stratosphere and weakening in the lower stratosphere (Fig. 12h). The changes in the residual circulation in the lower stratosphere drive a dynamical cooling trend over the polar cap (Fig. 13c) that, as in October, adds to the radiative cooling trend due to ozone depletion to produce a stronger negative temperature trend in Chem ON. The dynamical warming in the middle and upper polar stratosphere is also stronger in Chem ON, explaining the stronger warming trend in Fig. 9a.

The residual circulation in the lower stratosphere thus exhibits a different response to the formation of the ozone hole in Chem OFF compared to Chem ON. These different residual circulation changes are the consequence of the missing ozone-radiative-dynamical feedbacks in Chem OFF and of the resulting displacement of the ozone hole compared to the polar vortex. They are at the core of the temperature and westerly winds differences between the two ensembles, as they drive the dynamical heating contribution to the temperature changes.

4.3 Effects on the SAM timescale

Dennison et al. (2015) showed that ozone depletion increases the persistence of the SAM in the stratosphere. This raises the question of whether prescribing the CMIP6 ozone affects the impact of the ozone hole on the SAM persistence. Figure 14 shows the seasonal evolution of the ensemble mean SAM timescale for Chem ON and Chem OFF. The SAM timescale was

https://doi.org/10.5194/acp-2020-705
Preprint. Discussion started: 5 October 2020


Atmospheric Chemistry and Physics Discussions

first computed for the individual ensemble members and then averaged to obtain the ensemble means. While both Chem ON and Chem OFF capture the peak SAM persistence in austral spring and summer (Gerber et al., 2008, 2010), there are marked differences between the timescales in the two ensembles. The middle stratosphere SAM is more persistent in Chem ON between August and January, bringing the amplitude and the seasonal structure of the SAM timescale in Chem ON closer to that exhibited in reanalyses (compare Fig. 14 with Fig. 8b in the study by Gerber et al., 2010). In contrast, Chem OFF is characterized by a more vertical structure of the maximum persistence, focused in December, and, overall, by a shorter timescale. The inconsistent evolution of the ozone hole and the polar vortex in Chem OFF dampens the dynamical response to ozone depletion and reduces the SAM timescale. At the same time, the chemical-dynamical feedbacks present only in Chem ON reinforce the ozone-induced anomalies and lead to more persistent polar vortex anomalies, reflected in the longer SAM timescale in this ensemble. In a parallel study conducted with a different CCM by Haase et al. (2020), an ensemble of experiments with prescribed daily zonally asymmetric ozone consistent with the dynamics still exhibits shorter SAM timescales compared to the interactive chemistry experiment. This highlights the role of the feedbacks with the ozone chemistry in prolonging the SAM persistence. The same study additionally shows that the effect of zonal asymmetries in ozone is also to enhance the SAM timescale.

In the troposphere, both Chem ON and Chem OFF overestimate the SAM timescale and exhibit a peak persistence that is too broad when compared to the SAM timescale derived from reanalyses by Gerber et al. (2010) or Simpson et al. (2011). This is a common problem of climate models reported by Gerber et al. (2008) for the CMIP3 models and by Gerber et al. (2010) for CCMs and it appears to persist in the current generation of climate models. Simpson et al. (2011) attempted to identify the sources of the exaggerated tropospheric SAM persistence and found that the stratospheric SAM persistence contributes about half of the bias, while the other half is of tropospheric origin. The authors cite an equatorward-biased position of the tropospheric jet as a possible reason for the tropospheric contribution to the overestimation of the SAM timescale. This also holds true in our model, since the tropospheric jet in FOCI is located closer to the equator compared to observations, as it is common in climate models (Swart and Fyfe, 2012). Overall, the use of interactive chemistry improves the representation of the stratospheric SAM timescale in FOCI, but the tropospheric issues common to climate models still remain.

5 Discussion and conclusion

The ocean-atmosphere coupled climate model FOCI was used in this study to 1) separate the effects of ozone depletion on the SH temperature and dynamics from those arising from increasing concentrations of GHG and 2) to compare these effects between an ensemble of simulations where the CMIP6 ozone field is prescribed and an ensemble of simulations that use interactive chemistry. We found the following:

- The formation of the Antarctic ozone hole is the primary driver of the dynamical changes in the atmosphere that occurred in the SH spring and summer during the last decades. These changes comprise of an acceleration of the polar night jet, which propagated to the surface, where the surface westerlies shifted poleward and the SAM shifted toward its high index polarity.

https://doi.org/10.5194/acp-2020-705
Preprint. Discussion started: 5 October 2020


Atmospheric Chemistry and Physics Discussions

– The increase in anthropogenic GHG partly offset the November polar night jet response to ozone depletion in the stratosphere. At the surface, it resulted in a similar response of the westerlies and of the SAM, but this response was much weaker compared to that driven by ozone loss and it is generally not statistically significant.

– Ozone depletion drove an intensification of the SH BDC in the middle stratosphere in November and in the lower stratosphere in December. In contrast, a decrease in wave dissipation driven by ozone loss led to the weakening of the residual circulation in the lower stratosphere in November.

– The CMIP6 ozone field is not consistent with the dynamics simulated by FOCI and the ozone hole is not collocated with the polar vortex. Consequently, the austral spring zonal wavenumber one is weaker in Chem OFF and shifted eastwards compared to Chem ON. The austral spring climatological polar night jet is weaker in Chem OFF than in Chem ON.

– The dynamical response to ozone depletion enhanced the radiatively-driven austral spring lower stratospheric cooling. A novel result of this study is that this effect only occurs in Chem ON and it is suppressed in Chem OFF. Furthermore, the November lower stratosphere was dynamically warmed in Chem OFF, which partly offset the radiative cooling effect of ozone depletion.

– The SH atmospheric circulation response to ozone depletion is weaker in Chem OFF than in Chem ON. This is a consequence of the missing ozone-radiative-dynamical feedbacks and of the displacement of the ozone hole in relation to the polar vortex in Chem OFF, which alters the propagation of planetary waves from the troposphere and changes the location of suppressed wave breaking induced by the ozone hole. The ozone-induced spring lower stratospheric cooling in Chem ON is therefore closer to that reported from observations (e.g., Young et al., 2013).

– The persistence of the SAM is reduced in Chem OFF due to the dynamically-inconsistent prescribed ozone field, which represents another new result.

The temperature and dynamical response to ozone depletion simulated by FOCI is in good agreement with previous studies. The austral spring lower stratospheric cooling is the signature of the formation of the Antarctic ozone hole, a direct radiative effect also reported by Mahlman et al. (1994); Li et al. (2008); Stolarski et al. (2010); Keeble et al. (2014); Ivy et al. (2016) and Lubis et al. (2016). The November-December warming above the ozone hole represents a dynamical response to ozone loss and is in agreement with the findings of Mahlman et al. (1994); Li et al. (2008); Stolarski et al. (2010); Keeble et al. (2014) and Ivy et al. (2016). This confirms the ability of the model to accurately capture the stratospheric temperature response to ozone depletion. The strong and significant intensification of the polar night jet in austral spring and that of the surface westerlies in austral summer simulated by FOCI as a result of Antarctic ozone loss, combined with the weak and insignificant response of the surface westerlies to the increase in GHG, bring robustness to the conclusions of previous studies (Arblaster and Meehl, 2006; McLandress et al., 2010; Polvani et al., 2011; Previdi and Polvani, 2014; World Meteorological Organization, 2018) that ozone depletion is the main driver of SH stratospheric and tropospheric dynamical changes over the later part of the twentieth century. This is likely to change in the twenty first century, as even higher GHG levels will increase the GHG impact on the

https://doi.org/10.5194/acp-2020-705
Preprint. Discussion started: 5 October 2020


Atmospheric Chemistry and Physics Discussions

atmospheric circulation, while the ban on CFCs emissions following the Montreal protocol is expected to result in a recovery of the ozone hole, driving circulation changes in the opposite direction to those that occurred over the historical period (Perlwitz et al., 2008; Son et al., 2008; McLandress et al., 2010; Eyring et al., 2013).

The strengthening of the westerly winds in response to ozone depletion delayed the breakdown of the polar vortex, which allowed planetary waves to propagate higher into the stratosphere in November and for a longer period of time in December. This resulted in stronger wave dissipation in the upper stratosphere in November and in the middle stratosphere in December, leading to the concomitant intensification of the residual circulation, in agreement with the findings of previous studies that used CCMs (Li et al., 2008; McLandress et al., 2010; Li et al., 2010; Keeble et al., 2014; Oberländer-Hayn et al., 2015; Polvani et al., 2018; Abalos et al., 2019). A new result of this study is that the intensification of the residual circulation is weaker when the CMIP6 ozone field is prescribed and, furthermore, it extends farther down in the lower stratosphere in November. Chem OFF is not able to reproduce the November lower stratosphere residual circulation weakening found in Chem ON in agreement with other CCMs (Li et al., 2008; McLandress et al., 2010; Lubis et al., 2016). This is an essential aspect in explaining the weaker lower stratospheric cooling in response to ozone depletion in Chem OFF. The enhanced lower stratospheric polar cap downwelling results in dynamical warming, which reduces the radiative cooling due to ozone loss in November. The consequence is that Chem OFF exhibits a weaker spring lower stratospheric cooling compared to Chem ON and to several radiosonde-based observational products (Young et al., 2013).

The performance of simulations prescribing the CMIP6 ozone field was tested here for the first time against simulations that calculate the ozone chemistry interactively. To date, studies investigating the SH impact of prescribing instead of interactively calculating the ozone field have mainly focused on the effect of zonal asymmetries in ozone (Gillett et al., 2009; Waugh et al., 2009; Li et al., 2016; Rae et al., 2019) and of temporal interpolation (Sassi et al., 2005; Neely et al., 2014). Waugh et al. (2009) and Li et al. (2016) showed that the trends in the SH polar cap stratospheric temperature and in the stratospheric and tropospheric westerlies are weaker in the absence of zonal asymmetries in ozone. An important result of this study is that, despite prescribing ozone zonal asymmetries, these trends are still weaker in Chem OFF than in Chem ON and there are significant differences between the SH mean state between the two ensembles. These differences still persist due to the lack of feedbacks between ozone chemistry and dynamics and due to the inconsistencies between the prescribed ozone field and the simulated dynamics. The fact that the prescribed ozone hole is displaced in relation to the simulated polar vortex alters the propagation of planetary waves from the troposphere and ultimately results in the weaker temperature and circulation trends in Chem OFF. The monthly temporal resolution of the prescribed ozone field does not appear to play a role in these differences in FOCI. In a parallel study, Haase et al. (2020) analysed the effects of the missing ozone-radiative-dynamical feedbacks on the SH atmospheric circulation in simulations with a prescribed daily ozone field that was generated by the same model it was prescribed to. The important difference between the current study and that of Haase et al. (2020) is that the ozone field they prescribed is consitent with the model's dynamics, while the CMIP6 ozone field prescribed here is not. As shown above, this lack of consistency between ozone and dynamics leads to substantial differences in the simulated SH circulation response to ozone depletion. Our results suggest that the climate models participating in the current phase of the Coupled Model Intercomparison Project (CIMP6) that do not calculate the stratospheric ozone chemistry interactively will continue to

https://doi.org/10.5194/acp-2020-705
Preprint. Discussion started: 5 October 2020


Atmospheric Chemistry and Physics Discussions

underestimate the effects of ozone depletion on the SH circulation, and possibly those of ozone recovery, compared to CCMs. In our model, prescribing the CMIP6 ozone leads to an underestimation of about 23% in the austral spring lower stratospheric cooling trend between 1958 and 2013.

Data availability. The model data used in this study can be found at https://zenodo.org/record/3931507. The CMIP6 ozone field prescribed to the simulations that do not calculate the ozone chemistry interactively is publically available at http://blogs.reading.ac.uk/ccmi/forcing-databases-in-support-of-cmip6/.

Author contributions. II, KM and AB designed the study and the experimental set up. SW, II and JH carried out the model simulations. II carried out the analysis and all authors discussed the results. II wrote the manuscript with contributions from all co-authors.

Competing interests. The authors declare that they have no conflict of interest.

Acknowledgements. This study was funded by the German Federal Ministry of Education and Research (Bundesministerium für Bildung und Forschung - BMBF) through the SPACES-II CASISAC project, grant number 03F0796A. The model simulations were performed with resources provided by the North-German Supercomputing Alliance (HLRN). We thank Isla Simpson for her help in the calculation of the Southern Annular Mode timescale.

https://doi.org/10.5194/acp-2020-705
Preprint. Discussion started: 5 October 2020

Atmospheric Chemistry and Physics Discussions

References

Abalos, M., Polvani, L., Calvo, N., Kinnison, D., Ploeger, F., Randel, W., and Solomon, S.: New Insights on the Impact of Ozone-Depleting Substances on the Brewer-Dobson Circulation, Journal of Geophysical Research: Atmospheres, 124, 2435–2451, https://doi.org/10.1029/2018JD029301, 2019.

Andrews, D. G., Holton, J. R., and Leovy, C. B.: Middle Atmosphere Dynamics, vol. 40 of *International Geophysics Series*, Academic Press, 1987.

Arblaster, J. M. and Meehl, G. A.: Contributions of External Forcings to Southern Annular Mode Trends, Journal of Climate, 19, 2896–2905, https://doi.org/10.1175/JCLI3774.1, 2006.

Biastoch, A., Böning, C. W., Getzlaff, J., Molines, J.-M., and Madec, G.: Causes of Interannual–Decadal Variability in the Meridional Overturning Circulation of the Midlatitude North Atlantic Ocean, Journal of Climate, 21, 6599–6615, https://doi.org/10.1175/2008JCLI2404.1, 2008.

Biastoch, A., Böning, C. W., Schwarzkopf, F. U., and Lutjeharms, J. R. E.: Increase in Agulhas leakage due to poleward shift of Southern Hemisphere westerlies, Nature, 462, 495–498, https://doi.org/10.1038/nature08519, 2009.

Biastoch, A., Durgadoo, J. V., Morrison, A. K., van Sebille, E., Weijer, W., and Griffies, S. M.: Atlantic multi-decadal oscillation covaries with Agulhas leakage, Nature Communications, 6, 10 082, https://doi.org/10.1038/ncomms10082, 2015.

Brovkin, V., Raddatz, T., Reick, C. H., Claussen, M., and Gayler, V.: Global biogeophysical interactions between forest and climate, Geophysical Research Letters, 36, https://doi.org/10.1029/2009GL037543, 2009.

Cai, W.: Antarctic ozone depletion causes an intensification of the Southern Ocean super-gyre circulation, Geophysical Research Letters, 33, https://doi.org/10.1029/2005GL024911, 2006.

Charney, J. G. and Drazin, P. G.: Propagation of planetary-scale disturbances from the lower into the upper atmosphere, Journal of Geophysical Research (1896-1977), 66, 83–109, 1961.

Crook, J. A., Gillett, N. P., and Keeley, S. P. E.: Sensitivity of Southern Hemisphere climate to zonal asymmetry in ozone, Geophysical Research Letters, 35, https://doi.org/10.1029/2007GL032698, 2008.

Dennison, F. W., McDonald, A. J., and Morgenstern, O.: The effect of ozone depletion on the Southern Annular Mode and stratosphere-troposphere coupling, Journal of Geophysical Research: Atmospheres, 120, 6305–6312, https://doi.org/10.1002/2014JD023009, 2015.

Durgadoo, J. V., Loveday, B. R., Reason, C. J. C., Penven, P., and Biastoch, A.: Agulhas Leakage Predominantly Responds to the Southern Hemisphere Westerlies, Journal of Physical Oceanography, 43, 2113–2131, https://doi.org/10.1175/JPO-D-13-047.1, 2013.

Eyring, V., Arblaster, J. M., Cionni, I., Sedláček, J., Perlwitz, J., Young, P. J., Bekki, S., Bergmann, D., Cameron-Smith, P., Collins, W. J., Faluvegi, G., Gottschaldt, K.-D., Horowitz, L. W., Kinnison, D. E., Lamarque, J.-F., Marsh, D. R., Saint-Martin, D., Shindell, D. T., Sudo, K., Szopa, S., and Watanabe, S.: Long-term ozone changes and associated climate impacts in CMIP5 simulations, Journal of Geophysical Research: Atmospheres, 118, 5029–5060, https://doi.org/10.1002/jgrd.50316, 2013.

Fichefet, T. and Maqueda, M. A. M.: Sensitivity of a global sea ice model to the treatment of ice thermodynamics and dynamics, Journal of Geophysical Research: Oceans, 102, 12 609–12 646, https://doi.org/10.1029/97JC00480, 1997.

Fogt, R. L., Perlwitz, J., Monaghan, A. J., Bromwich, D. H., Jones, J. M., and Marshall, G. J.: Historical SAM Variability. Part II: Twentieth-Century Variability and Trends from Reconstructions, Observations, and the IPCC AR4 Models, Journal of Climate, 22, 5346–5365, https://doi.org/10.1175/2009JCLI2786.1, 2009.

https://doi.org/10.5194/acp-2020-705
Preprint. Discussion started: 5 October 2020

Fyfe, J. C., Boer, G. J., and Flato, G. M.: The Arctic and Antarctic oscillations and their projected changes under global warming, Geophysical Research Letters, 26, 1601–1604, https://doi.org/10.1029/1999GL900317, 1999.

Gabriel, A., Peters, D., Kirchner, I., and Graf, H.-F.: Effect of zonally asymmetric ozone on stratospheric temperature and planetary wave propagation, Geophysical Research Letters, 34, https://doi.org/10.1029/2006GL028998, 2007.

Garfinkel, C. I., Waugh, D. W., and Polvani, L. M.: Recent Hadley cell expansion: The role of internal atmospheric variability in reconciling modeled and observed trends, Geophysical Research Letters, 42, 10,824–10,831, https://doi.org/10.1002/2015GL066942, 2015.

Gerber, E. P., Polvani, L. M., and Ancukiewicz, D.: Annular mode time scales in the Intergovernmental Panel on Climate Change Fourth Assessment Report models, Geophysical Research Letters, 35, https://doi.org/10.1029/2008GL035712, 2008.

Gerber, E. P., Baldwin, M. P., Akiyoshi, H., Austin, J., Bekki, S., Braesicke, P., Butchart, N., Chipperfield, M., Dameris, M., Dhomse, S., Frith, S. M., Garcia, R. R., Garny, H., Gettelman, A., Hardiman, S. C., Karpechko, A., Marchand, M., Morgenstern, O., Nielsen, J. E., Pawson, S., Peter, T., Plummer, D. A., Pyle, J. A., Rozanov, E., Scinocca, J. F., Shepherd, T. G., and Smale, D.: Stratosphere-troposphere coupling and annular mode variability in chemistry-climate models, Journal of Geophysical Research: Atmospheres, 115, https://doi.org/10.1029/2009JD013770, 2010.

Gillett, N. P. and Thompson, D. W. J.: Simulation of Recent Southern Hemisphere Climate Change, Science, 302, 273–275, https://doi.org/10.1126/science.1087440, 2003.

Gillett, N. P., Scinocca, J. F., Plummer, D. A., and Reader, M. C.: Sensitivity of climate to dynamically-consistent zonal asymmetries in ozone, Geophysical Research Letters, 36, https://doi.org/10.1029/2009GL037246, 2009.

Grise, K. M., Polvani, L. M., Tselioudis, G., Wu, Y., and Zelinka, M. D.: The ozone hole indirect effect: Cloud-radiative anomalies accompanying the poleward shift of the eddy-driven jet in the Southern Hemisphere, Geophysical Research Letters, 40, 3688–3692, https://doi.org/10.1002/grl.50675, 2013.

Grytsai, A. V., Evtushevsky, O. M., Agapitov, O. V., Klekociuk, A. R., and Milinevsky, G. P.: Structure and long-term change in the zonal asymmetry in Antarctic total ozone during spring, Annales Geophysicae, 25, 361–374, 2007.

Haase, S. and Matthes, K.: The importance of interactive chemistry for stratosphere–troposphere coupling, Atmospheric Chemistry and Physics, 19, 3417–3432, https://doi.org/10.5194/acp-19-3417-2019, 2019.

Haase, S., Fricke, J., Kruschke, T., Wahl, S., and Matthes, K.: Sensitivity of the southern hemisphere tropospheric jet response to Antarctic ozone depletion: prescribed versus interactive chemistry, Atmospheric Chemistry and Physics Discussions, 2020, 1–33, https://doi.org/10.5194/acp-2020-441, 2020.

Haynes, P. H., McIntyre, M. E., Shepherd, T. G., Marks, C. J., and Shine, K. P.: On the "Downward Control" of Extratropical Diabatic Circulations by Eddy-Induced Mean Zonal Forces, Journal of the Atmospheric Sciences, 48, 651–678, https://doi.org/10.1175/1520-0469(1991)048<0651:OTCOED>2.0.CO;2, 1991.

Hegglin, M., Kinnison, D., Lamarque, J.-F., and Plummer, D.: CCMI ozone in support of CMIP6 - version 1.0, https://doi.org/10.22033/ESGF/input4MIPs.1115, 2016.

Ivy, D. J., Solomon, S., and Rieder, H. E.: Radiative and Dynamical Influences on Polar Stratospheric Temperature Trends, Journal of Climate, 29, 4927 – 4938, https://doi.org/10.1175/JCLI-D-15-0503.1, 2016.

Kang, S. M., Polvani, L. M., Fyfe, J. C., and Sigmond, M.: Impact of Polar Ozone Depletion on Subtropical Precipitation, Science, 332, 951–954, https://doi.org/10.1126/science.1202131, 2011.

https://doi.org/10.5194/acp-2020-705
Preprint. Discussion started: 5 October 2020

Keeble, J., Braesicke, P., Abraham, N. L., Roscoe, H. K., and Pyle, J. A.: The impact of polar stratospheric ozone loss on Southern Hemisphere stratospheric circulation and climate, Atmospheric Chemistry and Physics, 14, 13 705–13 717, https://doi.org/10.5194/acp-14-13705-2014, 2014.

Keeley, S. P. E., Gillett, N. P., Thompson, D. W. J., Solomon, S., and Forster, P. M.: Is Antarctic climate most sensitive to ozone depletion in the middle or lower stratosphere?, Geophysical Research Letters, 34, https://doi.org/10.1029/2007GL031238, 2007.

Kinnison, D. E., Brasseur, G. P., Walters, S., Garcia, R. R., Marsh, D. R., Sassi, F., Harvey, V. L., Randall, C. E., Emmons, L., Lamarque, J. F., Hess, P., Orlando, J. J., Tie, X. X., Randel, W., Pan, L. L., Gettelman, A., Granier, C., Diehl, T., Niemeier, U., and Simmons, A. J.: Sensitivity of chemical tracers to meteorological parameters in the MOZART-3 chemical transport model, Journal of Geophysical Research: Atmospheres, 112, https://doi.org/10.1029/2006JD007879, 2007.

Kushner, P. J., Held, I. M., and Delworth, T. L.: Southern Hemisphere Atmospheric Circulation Response to Global Warming, Journal of Climate, 14, 2238–2249, https://doi.org/10.1175/1520-0442(2001)014<0001:SHACRT>2.0.CO;2, 2001.

Langematz, U., Kunze, M., Krüger, K., Labitzke, K., and Roff, G. L.: Thermal and dynamical changes of the stratosphere since 1979 and their link to ozone and CO2 changes, Journal of Geophysical Research: Atmospheres, 108, ACL 9–1–ACL 9–13, https://doi.org/10.1029/2002JD002069, 2003.

Li, F., Austin, J., and Wilson, J.: The Strength of the Brewer-Dobson Circulation in a Changing Climate: Coupled Chemistry-Climate Model Simulations, Journal of Climate, 21, 40–57, https://doi.org/10.1175/2007JCLI1663.1, 2008.

Li, F., Newman, P. A., and Stolarski, R. S.: Relationships between the Brewer-Dobson circulation and the southern annular mode during austral summer in coupled chemistry-climate model simulations, Journal of Geophysical Research: Atmospheres, 115, https://doi.org/10.1029/2009JD012876, 2010.

Li, F., Vikhliaev, Y. V., Newman, P. A., Pawson, S., Perlwitz, J., Waugh, D. W., and Douglass, A. R.: Impacts of Interactive Stratospheric Chemistry on Antarctic and Southern Ocean Climate Change in the Goddard Earth Observing System, Version 5 (GEOS-5), Journal of Climate, 29, 3199–3218, https://doi.org/10.1175/JCLI-D-15-0572.1, 2016.

Li, F., Newman, P., Pawson, S., and Perlwitz, J.: Effects of Greenhouse Gas Increase and Stratospheric Ozone Depletion on Stratospheric Mean Age of Air in 1960-2010, Journal of Geophysical Research: Atmospheres, 123, 2098–2110, https://doi.org/10.1002/2017JD027562, 2018.

Lin, P., Fu, Q., Solomon, S., and Wallace, J. M.: Temperature Trend Patterns in Southern Hemisphere High Latitudes: Novel Indicators of Stratospheric Change, Journal of Climate, 22, 6325–6341, https://doi.org/10.1175/2009JCLI2971.1, 2009.

Lin, P., Paynter, D., Polvani, L., Correa, G. J. P., Ming, Y., and Ramaswamy, V.: Dependence of model-simulated response to ozone depletion on stratospheric polar vortex climatology, Geophysical Research Letters, 44, 6391–6398, https://doi.org/10.1002/2017GL073862, 2017.

Lubis, S. W., Omrani, N.-E., Matthes, K., and Wahl, S.: Impact of the Antarctic Ozone Hole on the Vertical Coupling of the Stratosphere–Mesosphere–Lower Thermosphere System, Journal of the Atmospheric Sciences, 73, 2509–2528, https://doi.org/10.1175/JAS-D-15-0189.1, 2016.

Madec, G. and the NEMO team: NEMO ocean engine - version 3.6, Note du Pôle de modélisation, Institut Pierre-Simon Laplace (IPSL), 2016.

Mahlman, J. D., Umscheid, L. J., and Pinto, J. P.: Transport, Radiative, and Dynamical Effects of the Antarctic Ozone Hole: A GFDL "SKYHI" Model Experiment, Journal of the Atmospheric Sciences, 51, 489–508, https://doi.org/10.1175/1520-0469(1994)051<0489:TRADEO>2.0.CO;2, 1994.

https://doi.org/10.5194/acp-2020-705
Preprint. Discussion started: 5 October 2020

Marshall, G. J.: Trends in the Southern Annular Mode from Observations and Reanalyses, Journal of Climate, 16, 4134–4143, https://doi.org/10.1175/1520-0442(2003)016<4134:TITSAM>2.0.CO;2, 2003.

Marshall, G. J., Stott, P. A., Turner, J., Connolley, W. M., King, J. C., and Lachlan-Cope, T. A.: Causes of exceptional atmospheric circulation changes in the Southern Hemisphere, Geophysical Research Letters, 31, https://doi.org/10.1029/2004GL019952, 2004.

Matthes, K., Funke, B., Andersson, M. E., Barnard, L., Beer, J., Charbonneau, P., Clilverd, M. A., Dudok de Wit, T., Haberreiter, M., Hendry, A., Jackman, C. H., Kretzschmar, M., Kruschke, T., Kunze, M., Langematz, U., Marsh, D. R., Maycock, A. C., Misios, S., Rodger, C. J., Scaife, A. A., Seppälä, A., Shangguan, M., Sinnhuber, M., Tourpali, K., Usoskin, I., van de Kamp, M., Verronen, P. T., and Versick, S.: Solar forcing for CMIP6 (v3.2), Geoscientific Model Development, 10, 2247–2302, https://doi.org/10.5194/gmd-10-2247-2017, 2017.

Matthes, K., Biastoch, A., Wahl, S., Harlaß, J., Martin, T., Brücher, T., Drews, A., Ehlert, D., Getzlaff, K., Krüger, F., Rath, W., Scheinert, M., Schwarzkopf, F. U., Bayr, T., Schmidt, H., and Park, W.: The Flexible Ocean and Climate Infrastructure Version 1 (FOCI1): Mean State and Variability, Geoscientific Model Development Discussions, 2020, 1–53, https://doi.org/10.5194/gmd-13-2533-2020, 2020.

McLandress, C. and Shepherd, T. G.: Simulated Anthropogenic Changes in the Brewer–Dobson Circulation, Including Its Extension to High Latitudes, Journal of Climate, 22, 1516–1540, https://doi.org/10.1175/2008JCLI2679.1, 2009.

McLandress, C., Jonsson, A. I., Plummer, D. A., Reader, M. C., Scinocca, J. F., and Shepherd, T. G.: Separating the Dynamical Effects of Climate Change and Ozone Depletion. Part I: Southern Hemisphere Stratosphere, Journal of Climate, 23, 5002–5020, https://doi.org/10.1175/2010JCLI3586.1, 2010.

McLandress, C., Shepherd, T. G., Scinocca, J. F., Plummer, D. A., Sigmond, M., Jonsson, A. I., and Reader, M. C.: Separating the Dynamical Effects of Climate Change and Ozone Depletion. Part II: Southern Hemisphere Troposphere, Journal of Climate, 24, 1850–1868, https://doi.org/10.1175/2010JCLI3958.1, 2011.

Meinshausen, M., Vogel, E., Nauels, A., Lorbacher, K., Meinshausen, N., Etheridge, D. M., Fraser, P. J., Montzka, S. A., Rayner, P. J., Trudinger, C. M., Krummel, P. B., Beyerle, U., Canadell, J. G., Daniel, J. S., Enting, I. G., Law, R. M., Lunder, C. R., O'Doherty, S., Prinn, R. G., Reimann, S., Rubino, M., Velders, G. J. M., Vollmer, M. K., Wang, R. H. J., and Weiss, R.: Historical greenhouse gas concentrations for climate modelling (CMIP6), Geoscientific Model Development, 10, 2057–2116, https://doi.org/10.5194/gmd-10-2057-2017, 2017.

Min, S.-K. and Son, S.-W.: Multimodel attribution of the Southern Hemisphere Hadley cell widening: Major role of ozone depletion, Journal of Geophysical Research: Atmospheres, 118, 3007–3015, https://doi.org/10.1002/jgrd.50232, 2013.

Neely, R. R., Marsh, D. R., Smith, K. L., Davis, S. M., and Polvani, L. M.: Biases in southern hemisphere climate trends induced by coarsely specifying the temporal resolution of stratospheric ozone, Geophysical Research Letters, 41, 8602–8610, https://doi.org/10.1002/2014GL061627, 2014.

North, G. R., Bell, T. L., Cahalan, R. F., and Moeng, F. J.: Sampling Errors in the Estimation of Empirical Orthogonal Functions, Monthly Weather Review, 110, 699–706, https://doi.org/10.1175/1520-0493(1982)110<0699:SEITEO>2.0.CO;2, 1982.

Oberländer-Hayn, S., Meul, S., Langematz, U., Abalichin, J., and Haenel, F.: A chemistry-climate model study of past changes in the Brewer-Dobson circulation, Journal of Geophysical Research: Atmospheres, 120, 6742–6757, https://doi.org/10.1002/2014JD022843, 2015.

Orr, A., Bracegirdle, T. J., Hosking, J. S., Jung, T., Haigh, J. D., Phillips, T., and Feng, W.: Possible Dynamical Mechanisms for Southern Hemisphere Climate Change due to the Ozone Hole, Journal of the Atmospheric Sciences, 69, 2917–2932, https://doi.org/10.1175/JAS-D-11-0210.1, 2012.

https://doi.org/10.5194/acp-2020-705
Preprint. Discussion started: 5 October 2020


Atmospheric Chemistry and Physics Discussions

Orr, A., Bracegirdle, T. J., Hosking, J. S., Feng, W., Roscoe, H. K., and Haigh, J. D.: Strong Dynamical Modulation of the Cooling of the Polar Stratosphere Associated with the Antarctic Ozone Hole, Journal of Climate, 26, 662–668, https://doi.org/10.1175/JCLI-D-12-00480.1, 2013.

Perlwitz, J., Pawson, S., Fogt, R. L., Nielsen, J. E., and Neff, W. D.: Impact of stratospheric ozone hole recovery on Antarctic climate, Geophysical Research Letters, 35, 10.1029/2008GL033 317, 2008.

Peters, D. H. W., Schneidereit, A., Bügelmayer, M., Zülicke, C., and Kirchner, I.: Atmospheric Circulation Changes in Response to an Observed Stratospheric Zonal Ozone Anomaly, Atmosphere-Ocean, 53, 74–88, https://doi.org/10.1080/07055900.2013.878833, 2015.

Polvani, L. M., Waugh, D. W., Correa, G. J. P., and Son, S.-W.: Stratospheric Ozone Depletion: The Main Driver of Twentieth-Century Atmospheric Circulation Changes in the Southern Hemisphere, Journal of Climate, 24, 795–812, https://doi.org/10.1175/2010JCLI3772.1, 2011.

Polvani, L. M., Abalos, M., Garcia, R., Kinnison, D., and Randel, W. J.: Significant Weakening of Brewer-Dobson Circulation Trends Over the 21st Century as a Consequence of the Montreal Protocol, Geophysical Research Letters, 45, 401–409, https://doi.org/10.1002/2017GL075345, 2018.

Previdi, M. and Polvani, L. M.: Climate system response to stratospheric ozone depletion and recovery, Quarterly Journal of the Royal Meteorological Society, 140, 2401–2419, https://doi.org/10.1002/qj.2330, 2014.

Rae, C. D., Keeble, J., Hitchcock, P., and Pyle, J. A.: Prescribing Zonally Asymmetric Ozone Climatologies in Climate Models: Performance Compared to a Chemistry-Climate Model, Journal of Advances in Modeling Earth Systems, 11, 918–933, https://doi.org/10.1029/2018MS001478, 2019.

Randel, W. J. and Wu, F.: Cooling of the Arctic and Antarctic Polar Stratospheres due to Ozone Depletion, Journal of Climate, 12, 1467–1479, https://doi.org/10.1175/1520-0442(1999)012<1467:COTAAA>2.0.CO;2, 1999.

Randel, W. J., Shine, K. P., Austin, J., Barnett, J., Claud, C., Gillett, N. P., Keckhut, P., Langematz, U., Lin, R., Long, C., Mears, C., Miller, A., Nash, J., Seidel, D. J., Thompson, D. W. J., Wu, F., and Yoden, S.: An update of observed stratospheric temperature trends, Journal of Geophysical Research: Atmospheres, 114, https://doi.org/10.1029/2008JD010421, 2009.

Reick, C. H., Raddatz, T., Brovkin, V., and Gayler, V.: Representation of natural and anthropogenic land cover change in MPI-ESM, Journal of Advances in Modeling Earth Systems, 5, 459–482, https://doi.org/10.1002/jame.20022, 2013.

Sassi, F., Boville, B. A., Kinnison, D., and Garcia, R. R.: The effects of interactive ozone chemistry on simulations of the middle atmosphere, Geophysical Research Letters, 32, https://doi.org/10.1029/2004GL022131, 2005.

Schultz, M. G., Stadtler, S., Schröder, S., Taraborrelli, D., Franco, B., Krefting, J., Henrot, A., Ferrachat, S., Lohmann, U., Neubauer, D., Siegenthaler-Le Drian, C., Wahl, S., Kokkola, H., Kühn, T., Rast, S., Schmidt, H., Stier, P., Kinnison, D., Tyndall, G. S., Orlando, J. J., and Wespes, C.: The chemistry-climate model ECHAM6.3-HAM2.3-MOZ1.0, Geoscientific Model Development, 11, 1695–1723, https://doi.org/10.5194/gmd-11-1695-2018, 2018.

Schwarzkopf, F. U., Biastoch, A., Böning, C. W., Chanut, J., Durgadoo, J. V., Getzlaff, K., Harlaß, J., Rieck, J. K., Roth, C., Scheinert, M. M., and Schubert, R.: The INALT family – a set of high-resolution nests for the Agulhas Current system within global NEMO ocean/sea-ice configurations, Geoscientific Model Development, 12, 3329–3355, https://doi.org/10.5194/gmd-12-3329-2019, 2019.

Simpson, I. R., Hitchcock, P., Shepherd, T. G., and Scinocca, J. F.: Stratospheric variability and tropospheric annular-mode timescales, Geophysical Research Letters, 38, https://doi.org/10.1029/2011GL049304, 2011.

Solomon, S.: Stratospheric ozone depletion: A review of concepts and history, Reviews of Geophysics, 37, 275–316, https://doi.org/10.1029/1999RG900008, 1999.

https://doi.org/10.5194/acp-2020-705
Preprint. Discussion started: 5 October 2020

Atmospheric Chemistry and Physics Discussions

Solomon, S., Kinnison, D., Bandoro, J., and Garcia, R.: Simulation of polar ozone depletion: An update, Journal of Geophysical Research: Atmospheres, 120, 7958–7974, https://doi.org/10.1002/2015JD023365, 2015.

Son, S.-W., Polvani, L. M., Waugh, D. W., Akiyoshi, H., Garcia, R., Kinnison, D., Pawson, S., Rozanov, E., Shepherd, T. G., and Shibata, K.: The Impact of Stratospheric Ozone Recovery on the Southern Hemisphere Westerly Jet, Science, 320, 1486–1489, https://doi.org/10.1126/science.1155939, 2008.

Son, S.-W., Polvani, L. M., Waugh, D. W., Birner, T., Akiyoshi, H., Garcia, R. R., Gettelman, A., Plummer, D. A., and Rozanov, E.: The Impact of Stratospheric Ozone Recovery on Tropopause Height Trends, Journal of Climate, 22, 429–445, https://doi.org/10.1175/2008JCLI2215.1, 2009.

Son, S.-W., Gerber, E. P., Perlwitz, J., Polvani, L. M., Gillett, N. P., Seo, K.-H., Eyring, V., Shepherd, T. G., Waugh, D., Akiyoshi, H., Austin, J., Baumgaertner, A., Bekki, S., Braesicke, P., Brühl, C., Butchart, N., Chipperfield, M. P., Cugnet, D., Dameris, M., Dhomse, S., Frith, S., Garny, H., Garcia, R., Hardiman, S. C., Jöckel, P., Lamarque, J. F., Mancini, E., Marchand, M., Michou, M., Nakamura, T., Morgenstern, O., Pitari, G., Plummer, D. A., Pyle, J., Rozanov, E., Scinocca, J. F., Shibata, K., Smale, D., Teyssèdre, H., Tian, W., and Yamashita, Y.: Impact of stratospheric ozone on Southern Hemisphere circulation change: A multimodel assessment, Journal of Geophysical Research: Atmospheres, 115, https://doi.org/10.1029/2010JD014271, 2010.

Stevens, B., Giorgetta, M., Esch, M., Mauritsen, T., Crueger, T., Rast, S., Salzmann, M., Schmidt, H., Bader, J., Block, K., Brokopf, R., Fast, I., Kinne, S., Kornblueh, L., Lohmann, U., Pincus, R., Reichler, T., and Roeckner, E.: Atmospheric component of the MPI-M Earth System Model: ECHAM6, Journal of Advances in Modeling Earth Systems, 5, 146–172, https://doi.org/10.1002/jame.20015, 2013.

Stolarski, R. S., Douglass, A. R., Newman, P. A., Pawson, S., and Schoeberl, M. R.: Relative Contribution of Greenhouse Gases and Ozone-Depleting Substances to Temperature Trends in the Stratosphere: A Chemistry–Climate Model Study, Journal of Climate, 23, 28–42, https://doi.org/10.1175/2009JCLI2955.1, 2010.

Swart, N. C. and Fyfe, J. C.: Observed and simulated changes in the Southern Hemisphere surface westerly wind-stress, Geophysical Research Letters, 39, https://doi.org/10.1029/2012GL052810, 2012.

Thompson, D. W. J. and Solomon, S.: Interpretation of Recent Southern Hemisphere Climate Change, Science, 296, 895–899, https://doi.org/10.1126/science.1069270, 2002.

Thompson, D. W. J., Solomon, S., Kushner, P. J., England, M. H., Grise, K. M., and Karoly, D. J.: Signatures of the Antarctic ozone hole in Southern Hemisphere surface climate change, Nature Geoscience, 4, 741–749, https://doi.org/10.1038/ngeo1296, 2011.

Waugh, D. W., Randel, W. J., Pawson, S., Newman, P. A., and Nash, E. R.: Persistence of the lower stratospheric polar vortices, Journal of Geophysical Research: Atmospheres, 104, 27 191–27 201, https://doi.org/10.1029/1999JD900795, 1999.

Waugh, D. W., Oman, L., Newman, P. A., Stolarski, R. S., Pawson, S., Nielsen, J. E., and Perlwitz, J.: Effect of zonal asymmetries in stratospheric ozone on simulated Southern Hemisphere climate trends, Geophysical Research Letters, 36, https://doi.org/10.1029/2009GL040419, 2009.

Waugh, D. W., Garfinkel, C. I., and Polvani, L. M.: Drivers of the Recent Tropical Expansion in the Southern Hemisphere: Changing SSTs or Ozone Depletion?, Journal of Climate, 28, 6581–6586, https://doi.org/10.1175/JCLI-D-15-0138.1, 2015.

World Meteorological Organization: Scientific Assessment of Ozone Depletion: 2018, Global Ozone Research and Monitoring Project–Report No. 58, Geneva, Switzerland, 2018.

Yang, X.-Y., Huang, R. X., and Wang, D. X.: Decadal Changes of Wind Stress over the Southern Ocean Associated with Antarctic Ozone Depletion, Journal of Climate, 20, 3395–3410, https://doi.org/10.1175/JCLI4195.1, 2007.

https://doi.org/10.5194/acp-2020-705
Preprint. Discussion started: 5 October 2020

Atmospheric Chemistry and Physics Discussions

Young, P. J., Butler, A. H., Calvo, N., Haimberger, L., Kushner, P. J., Marsh, D. R., Randel, W. J., and Rosenlof, K. H.: Agreement in late twentieth century Southern Hemisphere stratospheric temperature trends in observations and CCMVal-2, CMIP3, and CMIP5 models, Journal of Geophysical Research: Atmospheres, 118, 605–613, https://doi.org/10.1002/jgrd.50126, 2013.

https://doi.org/10.5194/acp-2020-705
Preprint. Discussion started: 5 October 2020

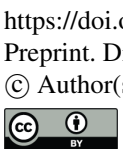

Atmospheric Chemistry and Physics Discussions

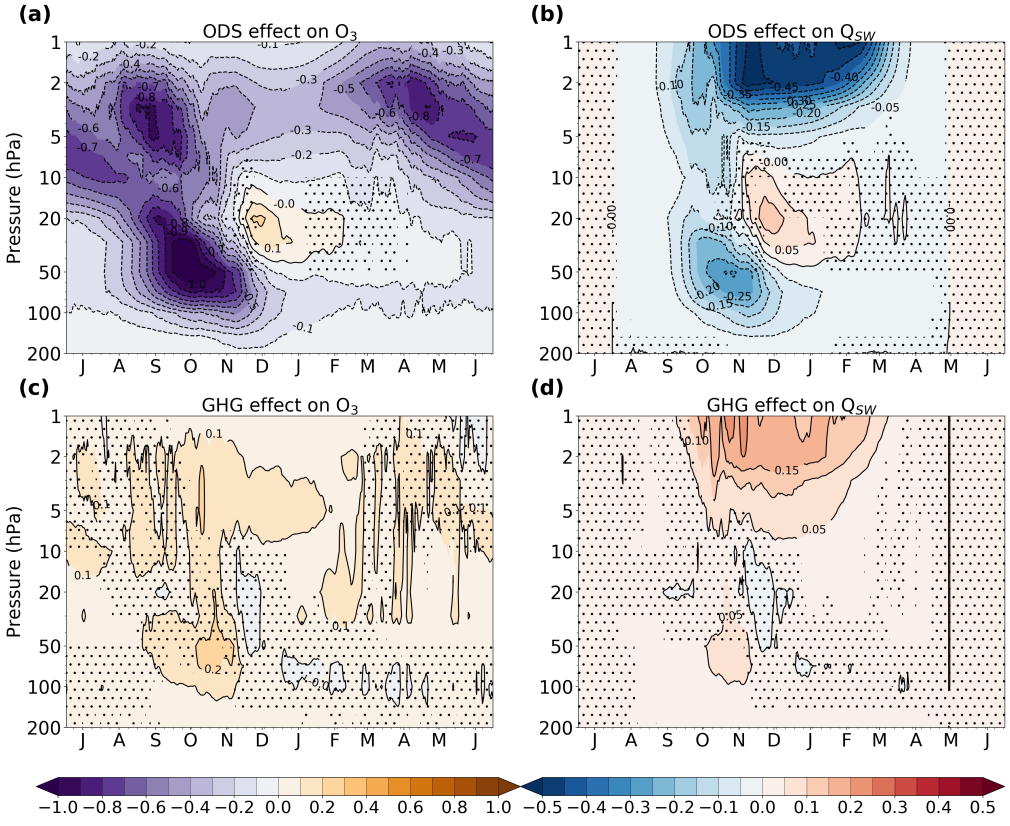

Figure 1. Seasonal cycle of the difference between REF and NoODS (a and b) and between REF and NoGHG (c and d) in the ozone volume mixing ratio (a and c, in ppmv) and the SW heating rate (b and d, in K day^{-1}) averaged over the polar cap (70°S-90°S) for the period 1958 – 2013. Stippling masks values that are not significant at the 95% confidence interval. The letter corresponding to each month marks the middle of that month.

https://doi.org/10.5194/acp-2020-705
Preprint. Discussion started: 5 October 2020

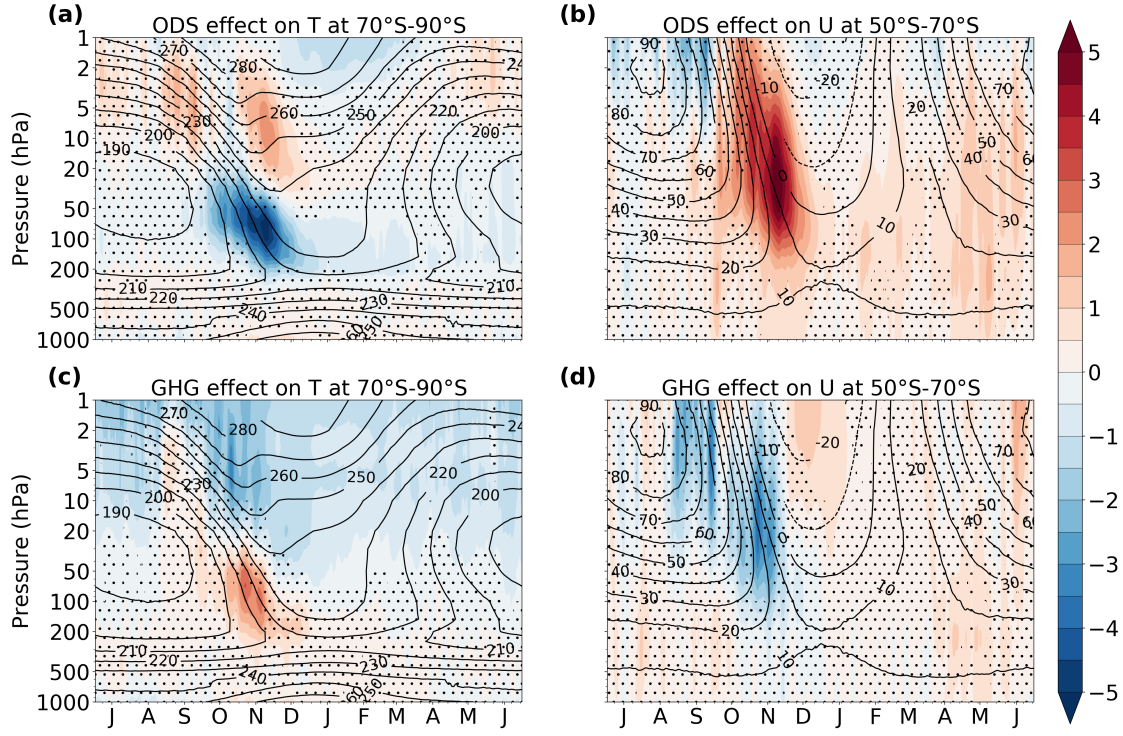

Figure 2. Seasonal cycle of the difference between REF and NoODS (a and b) and between REF and NoGHG (c and d) in the polar cap (70°S-90°S) temperature (a and c, in K) and in the mid-latitude (50°S-70°S) zonal wind (b and d, in $\mathrm{m\ s^{-1}}$) for the period 1958 – 2013 (color shading). Stippling masks values that are not significant at the 95% confidence interval. Contours show the corresponding climatological temperature and zonal wind from REF. The letter corresponding to each month marks the middle of that month.

https://doi.org/10.5194/acp-2020-705
Preprint. Discussion started: 5 October 2020

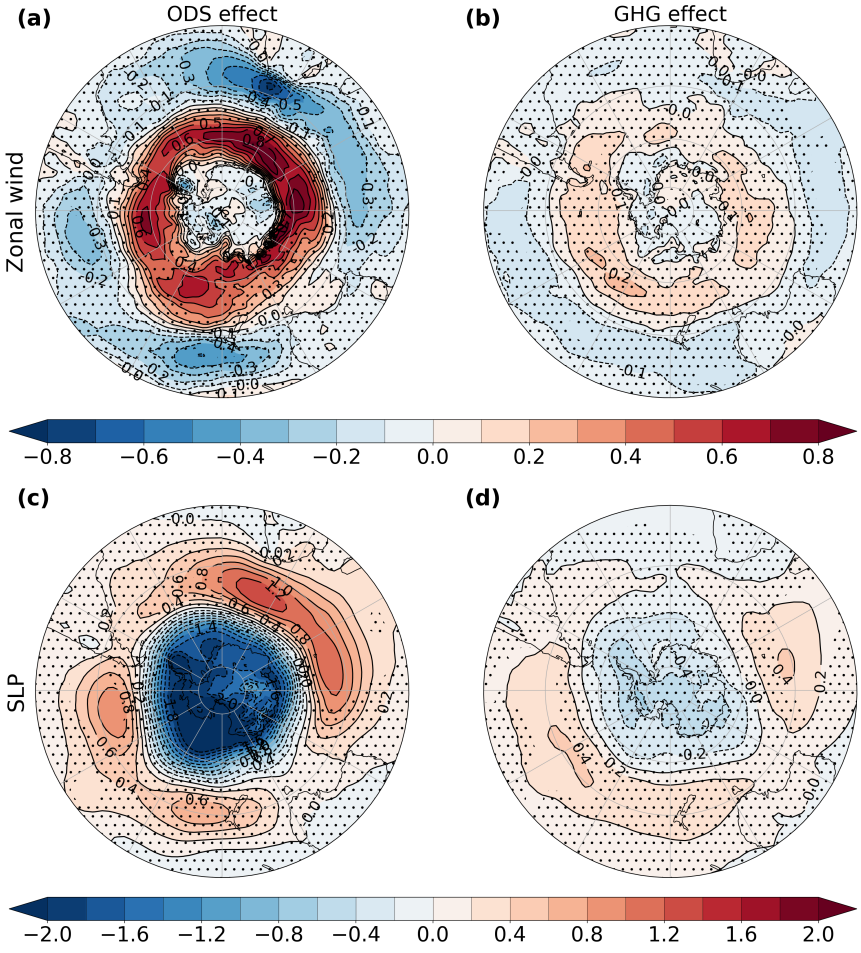

Figure 3. Polar stereographic maps of the November-December difference between REF and NoODS (a and c) and the annual mean difference between REF and NoGHG (b and d) in the surface zonal wind (a and b, in $\mathrm{m\ s^{-1}}$) and in sea level pressure (c and d, in hPa) for the period 1958 – 2013. Stippling masks values that are not significant at the 95% confidence interval.

https://doi.org/10.5194/acp-2020-705
Preprint. Discussion started: 5 October 2020

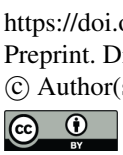

Atmospheric Chemistry and Physics Discussions

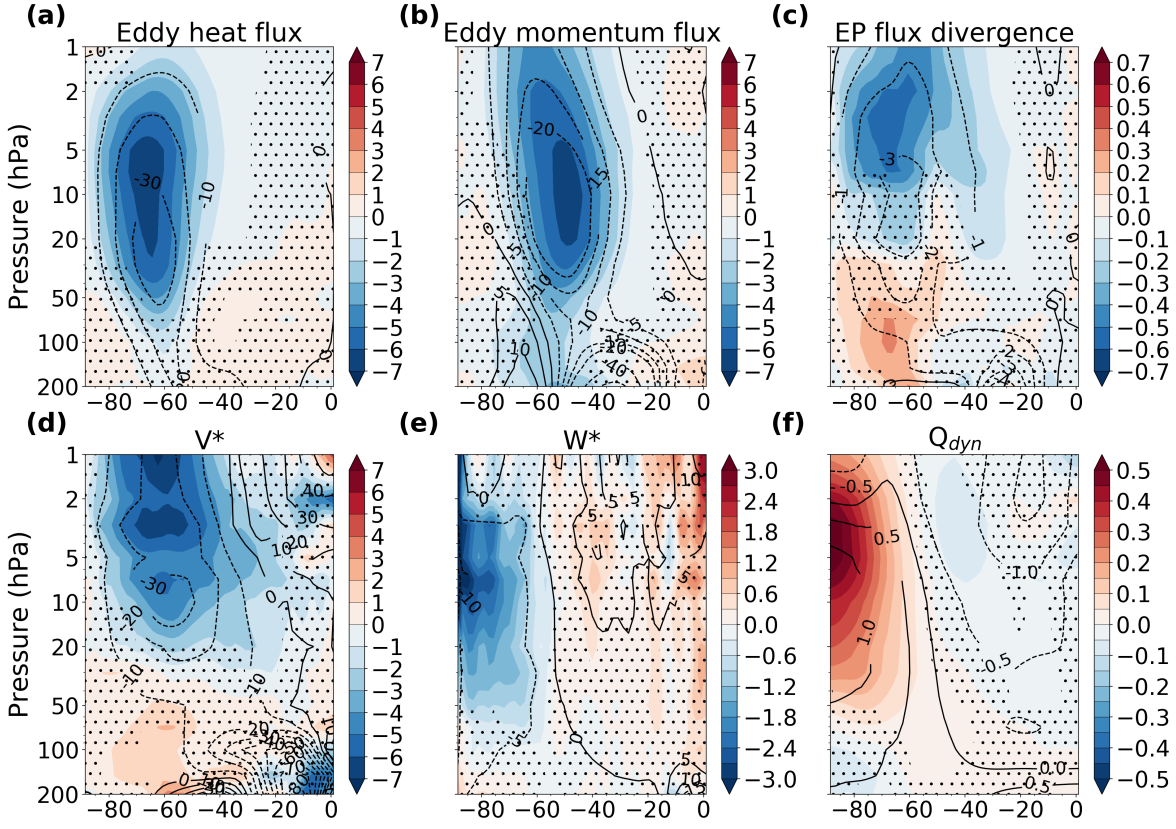

Figure 4. Latitude-height November difference between REF and NoODS in the eddy heat flux (a, in K $\mathrm{m\ s^{-1}}$), the eddy momentum flux (b, in $\mathrm{m^2 s^{-2}}$), the divergence of the EP flux (c, in $\mathrm{m\ s^{-1}\ day^{-1}}$), the meridional residual velocity (d, in $10^{-2}\mathrm{m\ s^{-1}}$), the vertical residual velocity (e, in $10^{-4}\mathrm{m\ s^{-1}}$) and in the dynamical heating rate (f, in K $\mathrm{day^{-1}}$) for the period 1958-2013 (color shading). Contours in each panel show the corresponding climatology from REF. Stippling masks values that are not significant at the 95% confidence interval.

https://doi.org/10.5194/acp-2020-705
Preprint. Discussion started: 5 October 2020

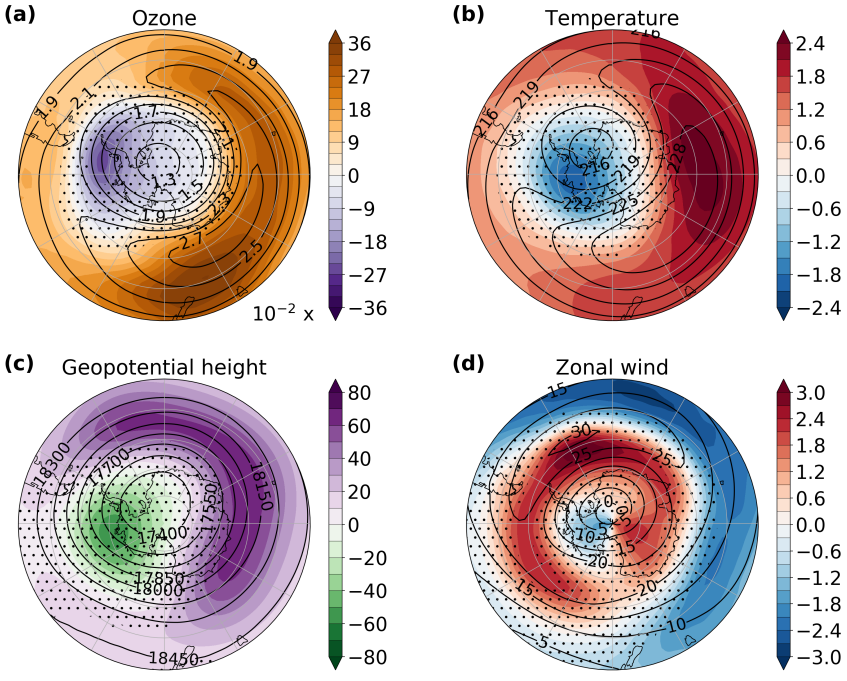

Figure 5. Polar stereographic maps of the difference between Chem ON and Chem OFF in the October mean ozone (a, in ppmv) and the November mean temperature (b, in K), geopotential height (c, in m) and zonal wind (d, in $\mathrm{m\ s^{-1}}$) at 70 hPa (color shading). The stippling masks regions that are not significant at the 95% confidence interval. The overlaying contours mark the 1958-2013 Chem ON climatology of each respective variable and month. Note that the scale in panel a is multiplied by 10^{-2}.

https://doi.org/10.5194/acp-2020-705
Preprint. Discussion started: 5 October 2020

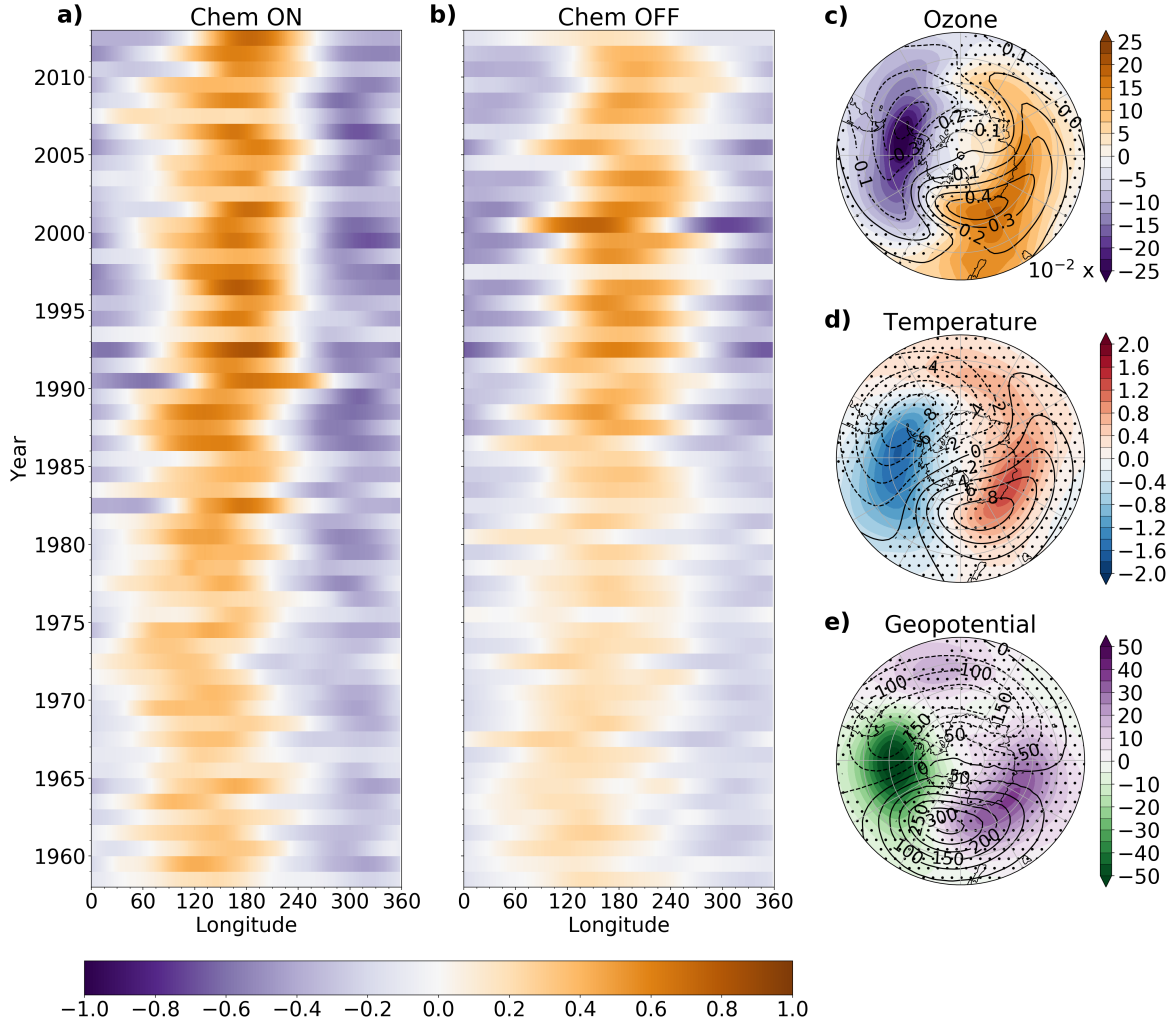

Figure 6. Hovmöller diagram of the October anomalies from the zonal mean ozone volume mixing ratio (in ppmv) in Chem ON (a) and Chem OFF (b) averaged over 60°S-70°S and maps of the October difference between Chem ON and Chem OFF in the anomalies from the zonal mean ozone volume mixing ratio (c, in ppmv), temperature (d, in K) and geopotential height (e, in m) at 70hPa for the period 1958-2013 (color shading). The stippling in panels c-e masks regions that are not significant at the 95% confidence interval. The overlaying contours mark the Chem ON 1958-2013 average anomalies from the zonal mean for each respective variable. Note that the scale in panel c is multiplied by 10^{-2}.

https://doi.org/10.5194/acp-2020-705
Preprint. Discussion started: 5 October 2020

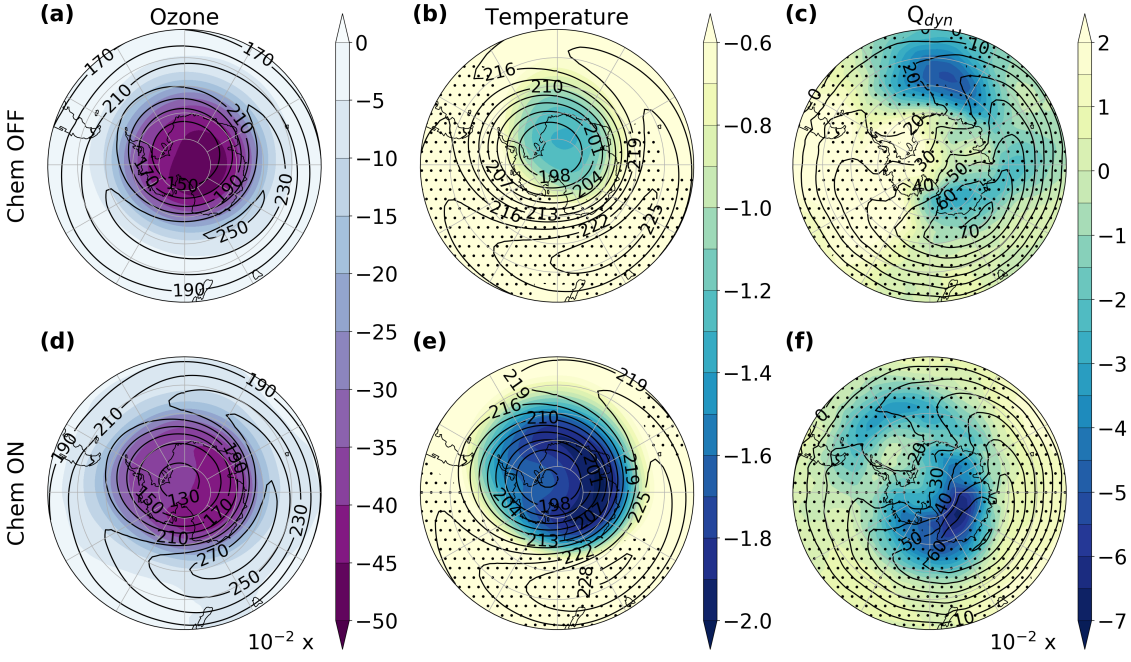

Figure 7. Polar stereographic maps of the October trends in ozone (a and d, in $\mathrm{ppmv\ dec^{-1}}$), temperature (b and e, in $\mathrm{K\ dec^{-1}}$) and dynamical heating rate (c and f, in $\mathrm{K\ day^{-1}\ dec^{-1}}$) at 70 hPa for Chem OFF (a, b and c) and Chem ON (d, e and f) over 1958-2013 (color shading). Stippling masks regions where the trends are not significant at the 95% confidence level. The overlaying contours show the respective October climatologies for 1958-2013. Note that the scales in panels a, c, d and f are multiplied by 10^{-2}.

https://doi.org/10.5194/acp-2020-705
Preprint. Discussion started: 5 October 2020

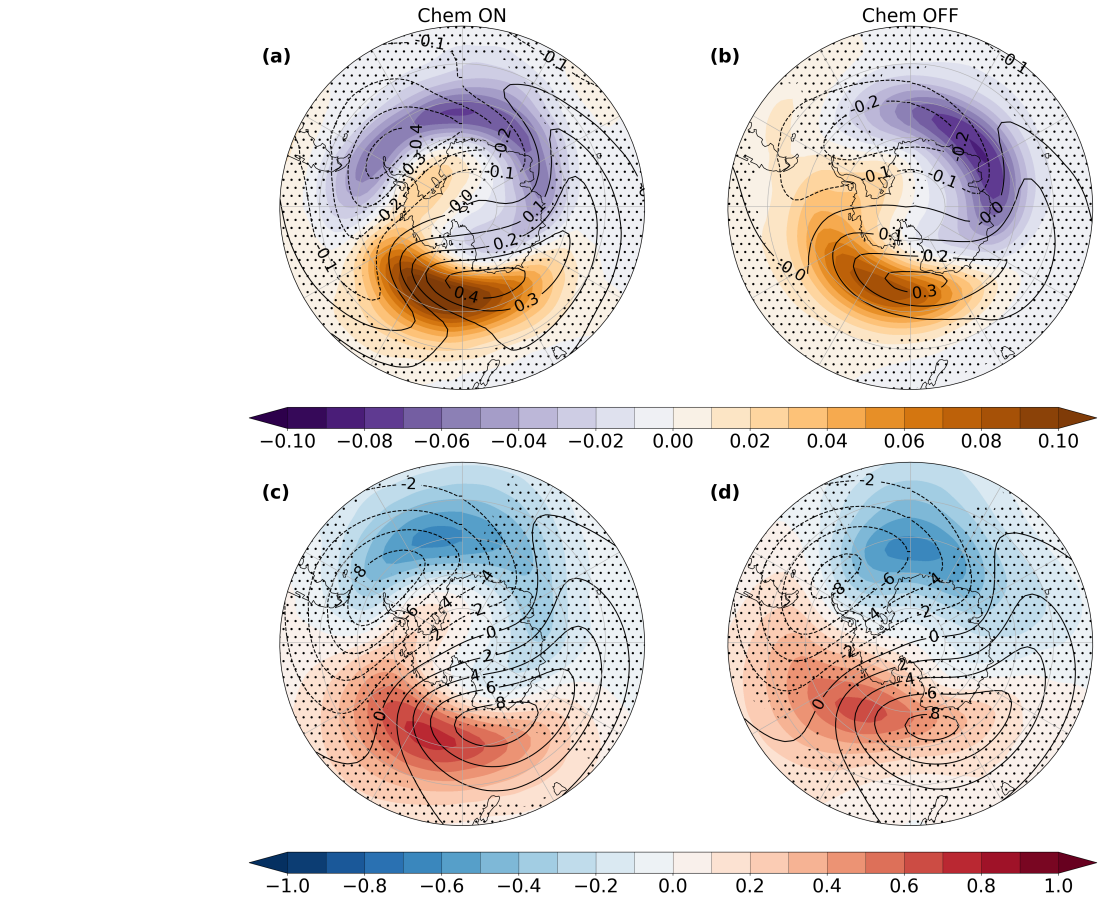

Figure 8. Polar stereographic maps of the October 70 hPa trends in Chem ON (a and c) and Chem OFF (b and d) ozone (a and b, in ppmv dec^{-1}) and temperature (c and d, in K dec^{-1}) anomalies from the zonal mean for the period 1958-2013 (color shading). Stippling masks regions where the trends are not significant at the 95% confidence level. The overlaying contours show the corresponding October climatologies.

https://doi.org/10.5194/acp-2020-705
Preprint. Discussion started: 5 October 2020

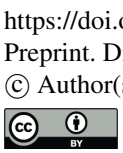

Atmospheric Chemistry and Physics Discussions

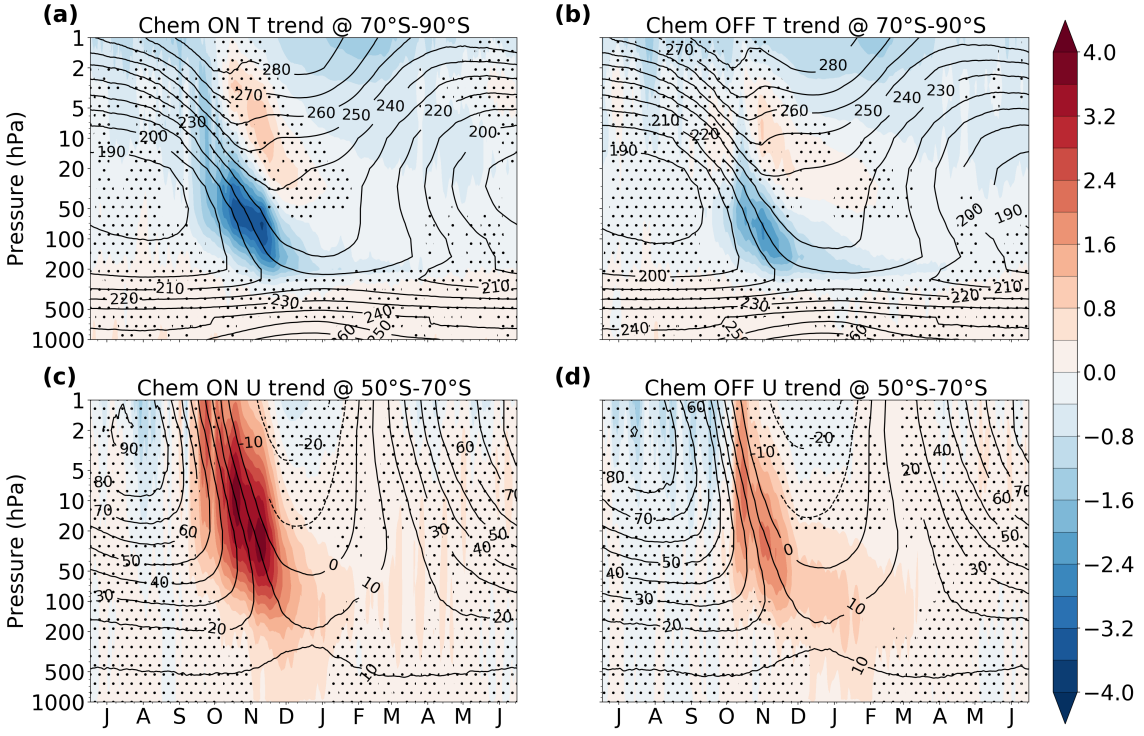

Figure 9. Seasonal cycle of the Chem ON (a and c) and Chem OFF (b and d) trends in polar cap (70°S-90°S) temperature (a and b, in K dec^{-1}) and in the mid-latitude (50°S-70°S) zonal wind (c and d, in $\mathrm{m\ s}^{-1}\ \mathrm{dec}^{-1}$) for the period 1958 – 2013 (color shading). Stippling masks regions where the trends are not significant at the 95% confidence level. The overlaying contours show the corresponding climatological seasonal cycle for 1958-2013. The letter corresponding to each month marks the middle of that month.

https://doi.org/10.5194/acp-2020-705
Preprint. Discussion started: 5 October 2020

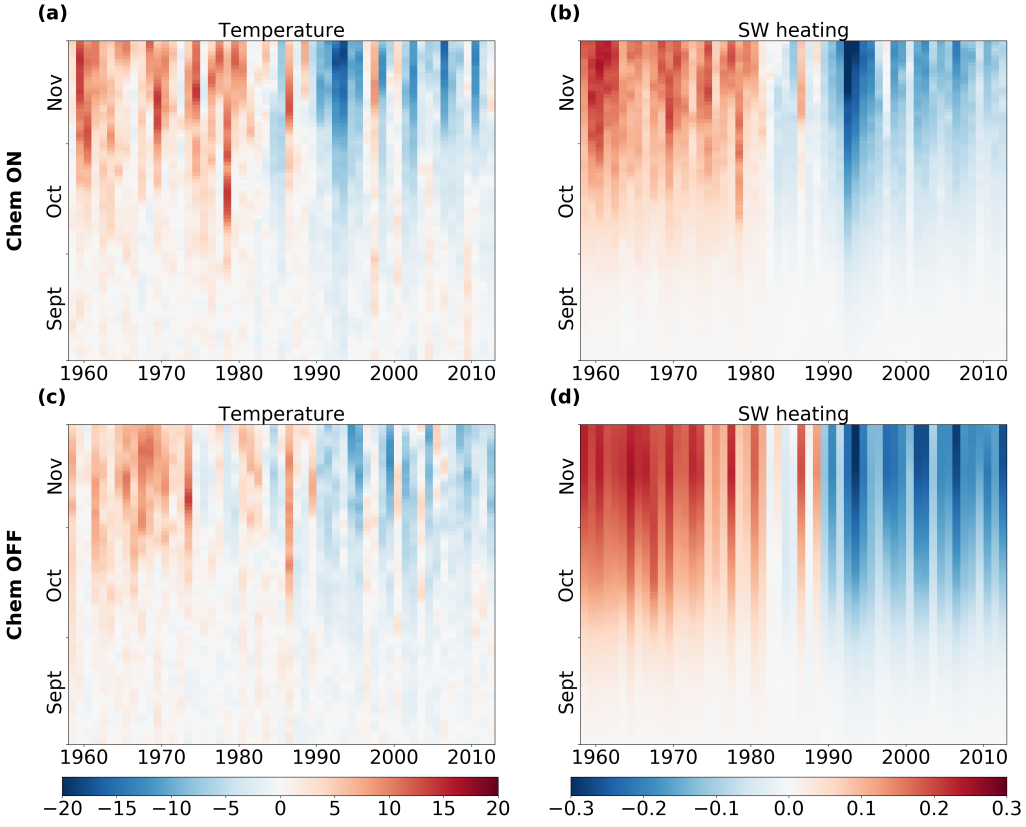

Figure 10. Timeseries of Chem ON (a, b) and Chem OFF (c, d) 100 hPa polar cap (70°S-90°S) temperature (a, c, in K) and SW heating rate (b, d, in K day^{-1}) anomalies with respect to the 1958-2013 climatology for each austral spring day.

https://doi.org/10.5194/acp-2020-705
Preprint. Discussion started: 5 October 2020

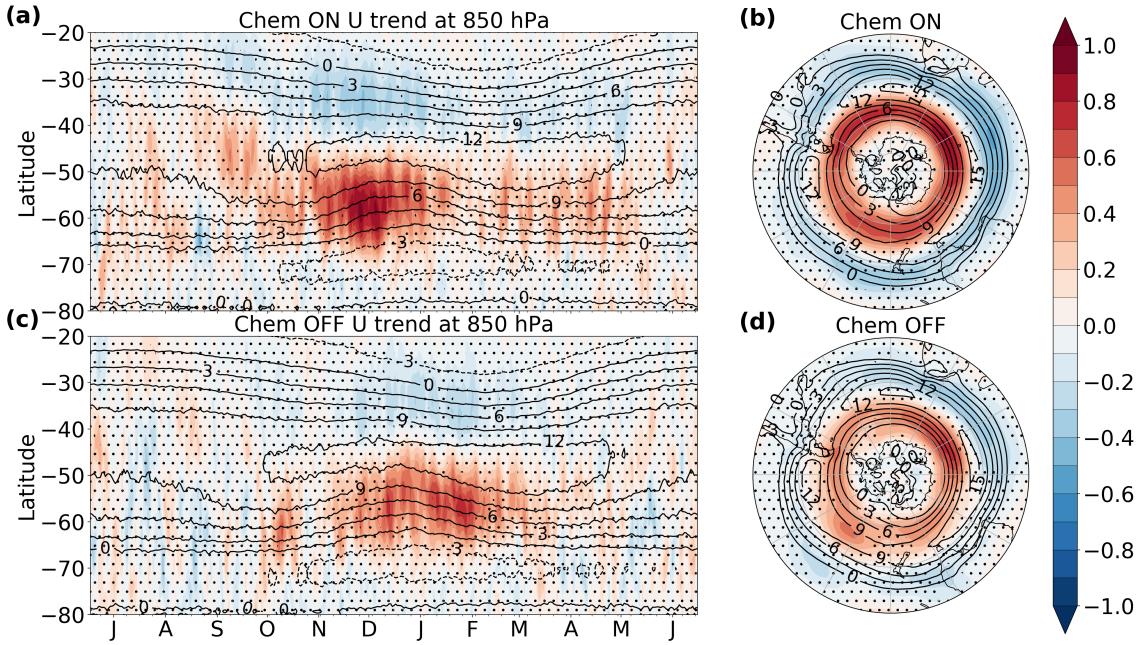

Figure 11. Seasonal cycle (a and c) and December-January polar stereographic maps (b and d) of the 850 hPa zonal wind trend (in $\mathrm{m\ s^{-1}\ dec^{-1}}$) in Chem ON (a and b) and Chem OFF (c and d) for the period 1958-2013 (color shading). Stippling masks regions where the trends are not significant at the 95% confidence level. The overlaying contours show the corresponding climatologies for 1958-2013. The letter corresponding to each month marks the middle of that month.

https://doi.org/10.5194/acp-2020-705
Preprint. Discussion started: 5 October 2020

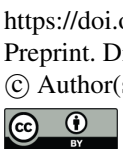

Atmospheric Chemistry and Physics Discussions

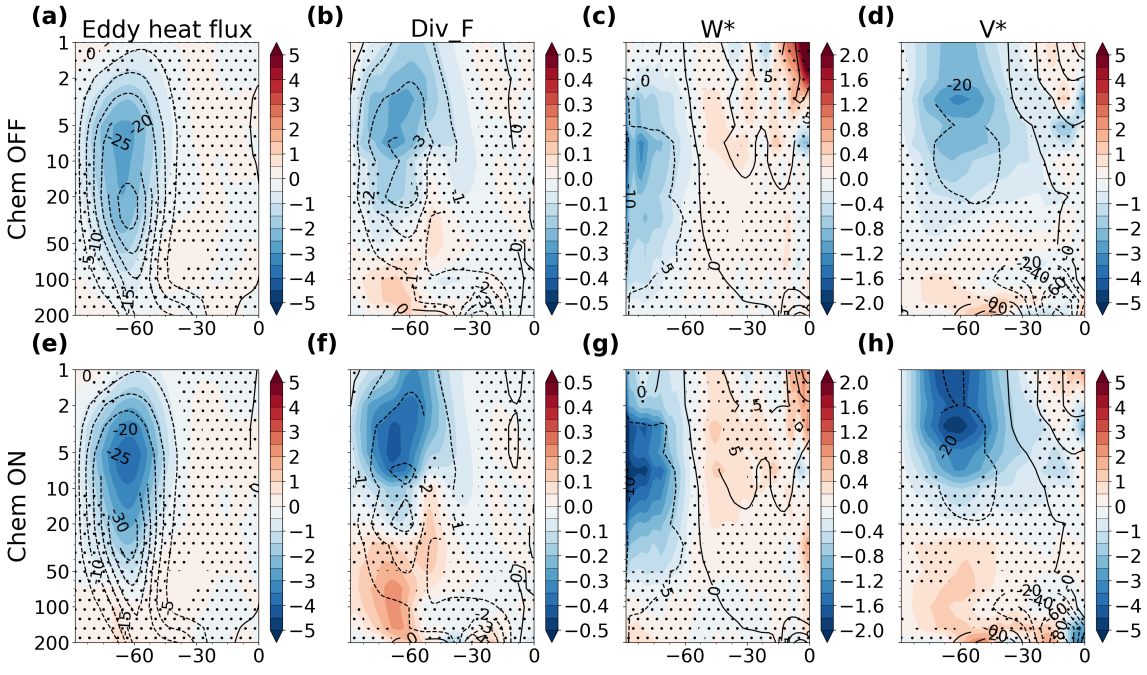

Figure 12. Latitude-height November trends in the eddy heat flux (a and e, in K m s^{-1} dec^{-1}), the divergence of the EP flux (b and f, in m $s^{-1}day^{-1}$ dec^{-1}), the vertical residual velocity (c and g, in 10^{-4} m s^{-1} dec^{-1}) and the meridional residual velocity (d and h, in 10^{-2} m s^{-1} dec^{-1}) for the period 1958-2013 in Chem OFF (a-d) and Chem ON (e-h). The overlaying contours in each panel show the corresponding climatologies. Stippling masks the trends that are not significant at the 95% confidence interval.

https://doi.org/10.5194/acp-2020-705
Preprint. Discussion started: 5 October 2020

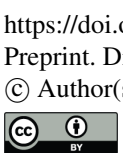

Atmospheric Chemistry and Physics Discussions

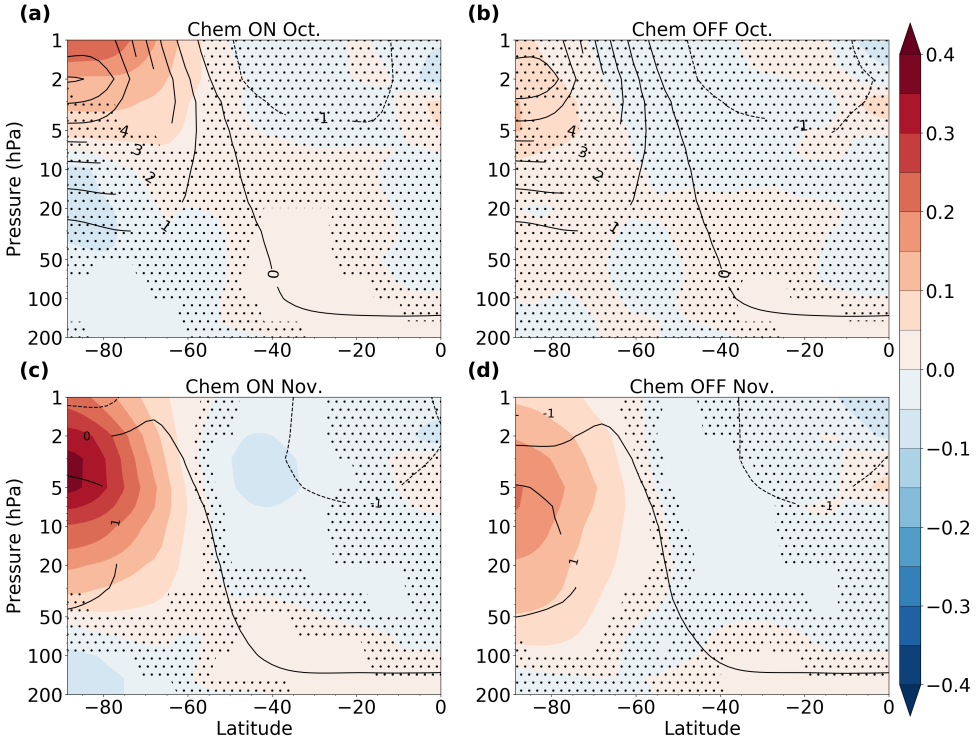

Figure 13. Latitude-height trends in October (a and b) and November (c and d) dynamical heating rate (in K day^{-1} dec^{-1}) in Chem ON (a and c) and Chem OFF (b and d) for the period 1958-2013 (color shading). Stippling masks the trends that are not significant at the 95% confidence interval. The overlaying contours in each panel show the corresponding climatologies.

https://doi.org/10.5194/acp-2020-705
Preprint. Discussion started: 5 October 2020

Atmospheric Chemistry and Physics Discussions

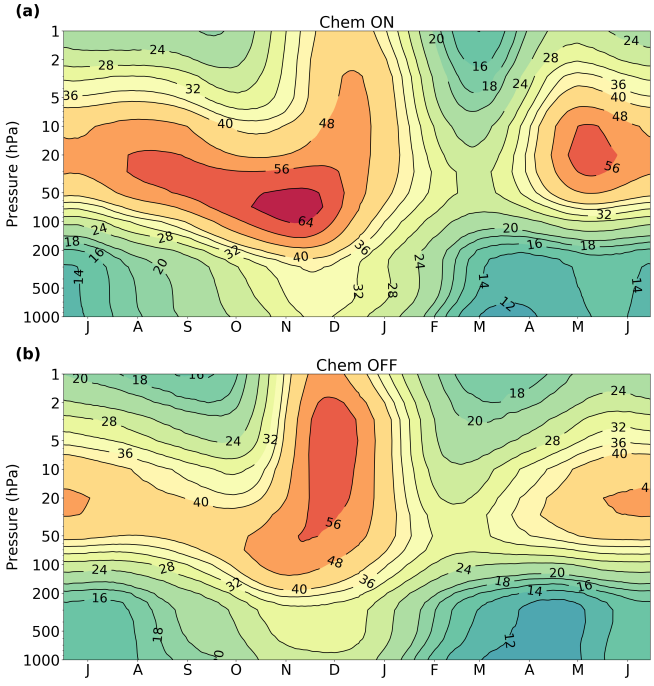

Figure 14. Seasonal cycle of the SAM timescale in Chem ON (a) and Chem OFF (b). Note that the contour interval is non-linear.

https://doi.org/10.5194/acp-2020-705
Preprint. Discussion started: 5 October 2020

Atmospheric Chemistry and Physics Discussions

Table 1. Overview of the FOCI ensembles used in this study. Each ensemble consists of 3 simulations which vary in their initial conditions.

Ensemble	Ozone chemistry	GHG	ODS	Analysis period
Chem OFF	prescribed CMIP6	historical CMIP6	historical CMIP6	1958-2013
Chem ON	interactive	historical CMIP6	historical CMIP6	1958-2013
REF	interactive	historical CMIP6	historical CMIP6	1958-2013
NoODS	interactive	historical CMIP6	fixed at 1960s level	1958-2013
NoGHG	interactive	fixed at 1960s level	historical CMIP6	1958-2013